Published in final edited form as:
Nat Immunol. 2020 March ; 21(3): 298–308. doi:10.1038/s41590-019-0589-5.

CD36-mediated metabolic adaptation supports regulatory T cell survival and function in tumors

Haiping Wang[1,2], **Fabien Franco**[1,2], **Yao-Chen Tsui**[1,2], **Xin Xie**[3], **Marcel P. Trefny**[4], **Roberta Zappasodi**[5,6], **Syed Raza Mohmood**[3], **Juan Fernández-García**[7,8], **Chin-Hsien Tsai**[1,2], **Isabell Schulze**[5,6], **Florence Picard**[1,2], **Etienne Meylan**[9], **Roy Silverstein**[10], **Ira Goldberg**[11], **Sarah-Maria Fendt**[7,8], **Jedd D. Wolchok**[5,6,12,13], **Taha Merghoub**[5,6,12], **Camilla Jandus**[1,2], **Alfred Zippelius**[4,14], **Ping-Chih Ho**[1,2]

[1]Department of Oncology, University of Lausanne, Switzerland [2]Ludwig Institute of Cancer Research, University of Lausanne, Switzerland [3]Center for Genomics and Systems Biology, NYU Abu Dhabi, United Arab Emirates [4]Department of Biomedicine, Laboratory Cancer Immunology, University Hospital and University of Basel, Switzerland [5]Ludwig Collaborative and Swiss Across America Laboratory, Memorial Sloan Kettering Cancer Center, USA [6]Parker Institute for Cancer Immunotherapy, Memorial Sloan Kettering Cancer Center, USA [7]Laboratory of Cellular Metabolism and Metabolic Regulation, VIB-KU Leuven Center for Cancer Biology, Belgium [8]Laboratory of Cellular Metabolism and Metabolic Regulation, Department of Oncology, KU Leuven and Leuven Cancer Institute, Belgium [9]Swiss Institute for Experimental Cancer Research School of Life Sciences, Ecole Polytechnique Fédérale de Lausanne, Switzerland [10]Department of Medicine, Medical College of Wisconsin, USA [11]Department of Medicine, NYU Langone Health, USA [12]Department of Medicine, Memorial Sloan Kettering Cancer Center, USA [13]Weill Cornell Medicine, USA [14]Medical Oncology, University Hospital Basel, Switzerland

Corresponding author: Ping-Chih Ho, Phone: 41-0-21-692-5947, Fax: 41-0-21-314-7477, ping-chih.ho@unil.ch.

Reporting Summary. Detailed information on experimental design is available in the Life Sciences Reporting Summary linked to this article.

Data availability

The RNA-seq data for intratumoral T_{reg} cells are available in the Gene Expression Omnibus database under accession code (GSE139325). All relevant data are available from the corresponding author upon request.

Author Contributions

H.W. and P.-C.H. contributed to overall project design and wrote manuscript. H.W., F.F., Y.-C.T., C.-H.T., and F.P. performed in vitro and in vivo animal works and data analysis. X.X. and S.R.M. performed analysis of RNA sequencing results. H.W., M.P.T., R.Z., J.D.W., T.M., C.J., I.S., and A.Z. conducted collection and flow cytometry analysis of human samples. J.F.G. and S.-M.F. supported metabolomite analysis. R.S. and I.G. provided the hybridoma clone for anti-CD36 antibody production and $CD36^{flox}$ mice, respectively. E.M. provided samples of NSCLC murine models.

Competing Interests Statement

H.W. and P.-C.H. are inventors of patent application related to targeting CD36 in cancer immunotherapy. P.-C.H. is serving as a member of scientific advisory board for Elixiron Immunotherapeutics and receiving research grants from Roche and Idorsia. J.D.W. is serving as a consultant for Adaptive Biotech; Advaxis; Amgen; Apricity; Array BioPharma; Ascentage Pharma; Astellas; Bayer; Beigene; Bristol Myers Squibb; Celgene; Chugai; Elucida; Eli Lilly; F Star; Genentech; Imvaq; Janssen; Kyowa Hakko Kirin; Kleo Pharma; Linneaus;MedImmune; Merck; Neon Therapuetics; Northern Biologics; Ono; Polaris Pharma; Polynoma; Psioxus; Puretech; Recepta; Takara Bio; Trieza; Sellas Life Sciences; Serametrix; Surface Oncology; Syndax; Synthologic. J.D.W. received research support from Bristol Myers Squibb; Medimmune; Merck Pharmaceuticals; Genentech and has equity in Potenza Therapeutics; Tizona Pharmaceuticals; Adaptive Biotechnologies; Elucida; Imvaq; Beigene; Trieza; Linneaus. P.C.H. received honorarium from Pfizer and Chugai and J.D.W received honorarium from Esanex.

Europe PMC Funders Author Manuscripts

Abstract

Depleting regulatory T cells (T_{reg} cells) to counteract immunosuppressive features of the tumor microenvironment (TME) is an attractive strategy for cancer treatment; however, autoimmunity due to systemic impairment of their suppressive function limits its therapeutic potential. Elucidating approaches that specifically disrupt intratumoral T_{reg} cells is direly needed for cancer immunotherapy. We found CD36 was selectively up-regulated in intrautumoral T_{reg} cells as a central metabolic modulator. CD36 fine-tuned mitochondrial fitness via PPAR-β signaling, programming T_{reg} cells to adapt to a lactic acid-enriched TME. Genetic ablation of *Cd36* in T_{reg} cells suppressed tumor growth accompanied by a decrease in intratumoral T_{reg} cells and enhancement of anti-tumor activity in tumor-infiltrating lymphocytes without disrupting immune homeostasis. Furthermore, CD36 targeting elicited additive anti-tumor responses with anti-PD-1 therapy. Our findings uncover the unexplored metabolic adaptation that orchestrate survival and functions of intratumoral T_{reg} cells, and the therapeutic potential of targeting this pathway for reprogramming the TME.

Introduction

Regulatory T (T_{reg}) cells are found at high frequencies in both mouse and human cancers[1–3], where they represent a major barrier to anti-tumor immunity and cancer immunotherapy[4,5]. While strategies depleting T_{reg} cells increase anti-tumor responses[6–8], the severe autoimmunity caused by systemic loss of T_{reg} cells and the unwanted depletion of effector T cells limit the therapeutic potential of Treg-targeting approaches. In addition, systemic impairment of suppressive functions in T_{reg} cells upon treatments targeting immune checkpoints, such as OX40, GITR and CTLA-4, expressing in T_{reg} cells also hampers the application of T_{reg} cell-targeting approaches in cancer treatment[9–11]. To date, the search for effective targeting approaches that selectively demolish intratumoral T_{reg} cells remains a challenge for cancer immunotherapy[12].

Progressive adaptation in transcriptome in T_{reg} cells migrating to barrier tissues has been revealed[13] and tissue context-dependent signals have been proposed to drive tissue-specific adaptation in T_{reg} cells without detailed understanding[14–20]. It also remains elusive whether the tissue context-dependent adaptation is required for proper functioning of peripheral T_{reg} cells. Emerging evidence reveals that metabolic machinery and nutrient-sensing mechanisms play critical roles to fine-tune proliferation, survival, suppressive function and lineage stability in T_{reg} cells[21–27]. Since the tumor microenvironment (TME) can impose a variety of types of metabolic stress on infiltrating immune cells[28], including acidosis, hypoxia, and nutrient deprivation, it is likely that intratumoral T_{reg} cells must adjust their metabolic preferences in response to these conditions as a consequence of adaptation to the TME. We therefore speculate that the metabolic adaptation engaged by intratumoral T_{reg} cells orchestrate signal pathways to support survival and suppressive activity.

We report here that intratumoral T_{reg} cells up-regulate CD36 expression to support mitochondrial fitness and biogenesis via a PPAR-β-dependent mechanism. Genetic ablation of *Cd36* in T_{reg} cells selectively abrogated the abundance and suppressive activity of intratumoral T_{reg} cells. Importantly, mice with genetic ablation of *Cd36* in T_{reg} cells did not

elicit autoimmunity and CD36-deficient splenic T_{reg} cells remained effective on restricting T cell transfer-induced colitis. Our results revealed that CD36-PPAR-β signal sustains survival and functional fitness in intratumoral T_{reg} cells by modulating mitochondrial fitness and NAD levels, which are critical for metabolizing lactate in the TME. We further provide proof-of-concept evidence that targeting CD36 with a monoclonal antibody induces superior anti-tumor immunity and elicits additive anti-tumor responses with anti-PD-1 treatment. These results highlight the unexplored CD36-PPAR-β-modulated metabolic adaptation, which allows intratumoral T_{reg} cells to utilize lactate in tumors, and suggest that targeting metabolic adaptation in intratumoral T_{reg} cells would be a promising strategy for reprogramming the TME without perturbing systemic immune and tissue homeostasis.

Results

Intratumoral T_{reg} cells increase lipid metabolism and CD36 expression

To elucidate whether intratumoral T_{reg} cells preferentially engage specific metabolic pathways, we first analyzed RNA-sequencing results from intratumoral and circulating T_{reg} cells obtained from breast cancer patients in a previously published study[29]. Gene pathway analysis, with a particular focus on metabolic pathways, revealed that intratumoral T_{reg} cells highly expressed metabolic genes responsible for lipid metabolism when compared to circulating T_{reg} cells (Fig. 1a,b), suggesting that intratumoral T_{reg} cells may increase their lipid metabolism. Indeed, when we compared peripheral blood mononuclear cells (PBMCs) and intratumoral T_{reg} cells from non-small-cell lung carcinoma (NSCLC) patients, intratumoral T_{reg} cells internalized a higher amount of a green fluorescent fatty acid, Bodipy FL C12, and contained a higher neutral lipid content based on the staining of Bodipy (Extended Data Fig. 1a,b). By examining T_{reg} cells in PBMCs and tumor-infiltrated lymph nodes (TILN) from melanoma patients, we also confirmed that intratumoral T_{reg} cells from the majority of patients internalized a higher amount of Bodipy FL C12 (Extended Data Fig. 1c); however, T_{reg} cells in both PBMCs and tumor-infiltrated lymph nodes (TILNs) contained similar lipid content (Extended Data Fig. 1d). To further explore these phenotypes, we used melanoma cell engraftment models to assess lipid metabolism in T_{reg} cells residing in tumors and other peripheral tissues. Intratumoral T_{reg} cells displayed an elevated ability to take up fatty acids (Fig. 1c) and had a higher lipid content (Fig. 1d) compared to T_{reg} cells from other tissues of YUMM1.7 melanoma-bearing mice. Similarly, intratumoral T_{reg} cells of B16 melanoma-bearing mice and MC38 colon carcinoma-bearing mice also exhibited enhanced fatty acid uptake (Extended Data Fig. 1e,f). These observations suggest that the increase in lipid metabolism, especially lipid uptake, by intratumoral T_{reg} cells is a conserved phenotype in both human and murine models. Of note, among genes controlling lipid uptake, *Cd36*, encoding a scavenger receptor responsible for long chain fatty acid and oxidized low-density lipoprotein uptake, was significantly up-regulated in intratumoral T_{reg} cells compared to circulating T_{reg} cells from breast cancer patients[29]. By examining T_{reg} cells in PBMCs and TILNs from melanoma patients, we confirmed that intratumoral T_{reg} cells from the majority of patients expressed higher amounts of CD36 (Fig. 1e). In addition, we found that intratumoral T_{reg} cells, but not T_{reg} cells residing in other peripheral tissues or secondary lymphoid organs from Yumm1.7 melanoma-bearing mice, expressed abundant CD36 (Fig. 1f). The increased expression of

CD36 found in intratumoral T_{reg} cells was also observed in NSCLC patients, as well as in the mouse B16 melanoma model, a genetically engineered Braf/PTEN melanoma mouse model, a *K-ras*$^{LSL\text{-}G12D/+}$/*p53*$^{fl/fl}$ conditional mouse model of NSCLC, and a MC38 colon carcinoma model (Extended Data Fig. 1g-k). Furthermore, we found that culturing inducible T_{reg} cells (iT_{reg} cells) in conditioned medium obtained from cancer cell cultures substantially increased CD36 expression, while hypoxia and lactic acid failed to induce CD36 expression in T_{reg} cells (Extended Data Fig. 1l). Lipid removal abolished the effects of cancer cell-conditioned media on stimulating CD36 expression in T_{reg} cells (Extended Data Fig. 1m). Together, our results suggest that the TME can stimulate CD36 expression in T_{reg} cells, which might support the demands for metabolic adaptation in intratumoral T_{reg} cells.

CD36 controls the accumulation and suppressive function of intratumoral T_{reg} cells

To investigate whether the expression of CD36 modulates Treg behavior in tumors, we generated T_{reg} cell-specific CD36-deficient mice (designated $T_{reg}^{Cd36-/-}$) by crossing *Cd36*$^{fl/fl}$ mice with *Foxp3*$^{YFP\text{-}Cre}$ mice. Given that genetic ablation of critical regulators in T_{reg} cells could lead to systemic activation of T lymphocytes and autoimmunity due to impairment of T_{reg} cell suppressive functions, we first examined whether deficiency of CD36 in T_{reg} cell impacts immune homeostasis. We found that aged $T_{reg}^{Cd36-/-}$ mice (21-23 weeks) displayed comparable body weights to *Foxp3*$^{YFP\text{-}Cre}$ mice (referred to wild-type mice throughout this study) in both genders (Extended Data Fig. 2a). $T_{reg}^{Cd36-/-}$ mice also contained a similar proportion of effector or memory population ($CD44^{hi}CD62L^{lo}$) in both $CD4^+$ and $CD8^+$ T cell compartments compared to wild-type mice (Extended Data Fig. 2b). Moreover, $T_{reg}^{Cd36-/-}$ mice showed neither abnormal infiltration of lymphocytes and myeloid cells in various organs nor severe systemic inflammatory disorders (Fig. 2a and Extended Data Fig. 2c), suggesting that CD36 is not required for T_{reg} cells to maintain immune homeostasis. We then engrafted YUMM1.7 melanoma cells into wild-type and $T_{reg}^{Cd36-/-}$ mice. We found that genetic ablation of *Cd36* in T_{reg} cells severely decreased lipid uptake and content in intratumoral T_{reg} cells, but not splenic T_{reg} cells (Fig. 2b,c), indicating that intratumoral T_{reg} cells rely on CD36 expression to support enhanced lipid uptake. We also observed growth deceleration of engrafted YUMM1.7 melanoma (Fig. 2d,e), B16 melanoma (Extended Data Fig. 2d), and MC38 colon carcinoma (Extended Data Fig. 2e) in $T_{reg}^{Cd36-/-}$ mice. Moreover, $T_{reg}^{Cd36-/-}$ mice had a profound loss of intratumoral T_{reg} cells, but not T_{reg} cells in spleen and draining lymph nodes at the end point of analyses (Fig. 2f and Extended Data Fig. 2f). This was accompanied by a significant increase in the frequency of $CD8^+$ tumor-infiltrating lymphocytes (TILs) as well as the ratio of intratumoral $CD8^+$ to T_{reg} cells (Extended Data Fig. 2g,h), a favorable parameter associated with strong anti-tumor responses. In addition, a higher frequency of $CD8^+$ TILs and $CD4^+FoxP3^-$ TILs in $T_{reg}^{Cd36-/-}$ mice produced anti-tumor effector cytokines, including interferon-γ (IFN-γ) and tumor necrosis factor (TNF) (Fig. 2g and Extended Data Fig. 2i), suggesting that the TME of $T_{reg}^{Cd36-/-}$ mice is less immunosuppressive. To further validate the dependency of CD36 on supporting accumulation of intratumoral T_{reg} cells, we generated heterozygous *Foxp3*$^{YFP\text{-}Cre/+}$*Cd36*$^{fl/fl}$ female mice, which simultaneously harbor a wild-type T_{reg} population and a CD36-deficient T_{reg} population driven by FoxP3 expression mediated by X chromosome inactivation. The wild-type and CD36-deficient T_{reg} cells can be detected on

the basis of the expression of yellow fluorescent protein (YFP). To exclude the potential toxicity induced by Cre recombinase, we also generated heterozygous *Foxp3*$^{YFP\text{-}Cre/+}$ female mice as control mice. By comparing YFP$^+$ populations among FoxP3$^+$ T_{reg} cells in both tumor-bearing *Foxp3*$^{YFP\text{-}Cre/+}$*Cd36*$^{fl/fl}$ and *Foxp3*$^{YFP\text{-}Cre/+}$ female mice, we only detected a reduction in frequencies of CD36-deficient T_{reg} cells (Cre$^+$ population in *Foxp3*$^{YFP\text{-}Cre/+}$*Cd36*$^{fl/fl}$ mice) in tumors, whereas the frequency ratios between Cre$^+$ and Cre$^-$ T_{reg} cells in both spleens and draining lymph nodes were comparable between *Foxp3*$^{YFP\text{-}Cre/+}$*Cd36*$^{fl/fl}$ and *Foxp3*$^{YFP\text{-}Cre/+}$ mice (Fig. 2h). This result suggested that loss of CD36 expression selectively perturb accumulation of intratumoral T_{reg} cells via intrinsic regulation. Altogether, these results reveal a crucial role for CD36 in selectively endowing T_{reg} cells with the ability to accumulate in the TME.

CD36 is dispensable in T_{reg} cells for maintaining periphery homeostasis

Intriguingly, we also found that intratumoral effector T_{reg} cells (CD44^{hi}CD62L^{lo}) exhibited higher expression of CD36 compared to intratumoral CD44^{lo} T_{reg} cells (resting T_{reg} cells) in murine melanoma model (Fig. 3a). Similarly, a higher percentage of tumor-infiltrating GITR$^+$CD25$^+$ effector T_{reg} cells, the most suppressive subset of effector T_{reg} cells[30,31], from TILs of melanoma patients expressed CD36 compared to GITR$^+$CD25$^+$ effector T_{reg} cells in PBMCs from melanoma patients and healthy donors (Fig. 3b). We next examined the expression of immunomodulatory receptors in intratumoral T_{reg} cells and found that CD36-deficient T_{reg} cells reduced the expression of glucocorticoid-induced TNFR-related protein (GITR) and OX40 (Fig. 3c,d), but not programmed cell death protein 1 (PD-1), CD25, cytotoxic T-lymphocyte-associated protein 4 (CTLA-4), or inducible T-cell costimulator (ICOS), compared to wild-type T_{reg} cells (Fig. 3e-h). These results suggest that CD36 expression contributes to the suppressive functions of effector T_{reg} cells. In support of this notion, we found that intratumoral T_{reg} cells from $T_{reg}^{Cd36\text{-}/\text{-}}$ mice displayed reduced suppressive capacity compared to wild-type intratumoral T_{reg} cells in the *ex vivo* suppressive assay (Fig. 3i). However, wild-type and CD36-deficient splenic T_{reg} cells displayed comparable suppressive capacity (Fig. 3j), suggesting that CD36 is only required for supporting suppressive activity of intratumoral T_{reg} cells, but not splenic T_{reg} cells. To further examine if CD36 is dispensable for T_{reg} cells to restraint peripheral inflammation, we analyzed the ability of CD36-deficient T_{reg} cells on suppressing T cell transfer-induced colitis. Disease onset such as weight loss was detected at two weeks post naïve CD4$^+$ T cell transfer. However, co-transferring CD36-deficient T_{reg} cells was able to ameliorate weight loss in the recipient mice comparably to wild-type T_{reg} cells (Fig. 3k). Moreover, several organs were removed at the study endpoint and processed for further evaluation by histology. Compared with naïve CD4$^+$ T cell transfer, which triggered massive infiltration of lymphocytes and myeloid cells, co-transfer of either wild-type or CD36-deficient T_{reg} cells impeded infiltration of lymphocytes and myeloid cells as well as morphology changes in colon and small intestine, colon shortening, and enlargement of spleen in the recipient mice (Fig. 3l and Extended Data Fig. 3a,b). Furthermore, we found that genetic ablation of *Cd36* neither affects the expression of activation markers, including CD44, CD103 and KLRG1 (Extended Data Fig. 3c-e), nor FoxP3 expression (indicated by the fluorescence intensity of YFP) (Extended Data Fig. 3f) in intratumoral T_{reg} cells. However, *CD36*-deficient intratumoral T_{reg} cells slightly enhanced the production of pro-inflammatory cytokines IFN-

γ and TNF (Extended Data Fig. 3g-i), suggesting that CD36 restraints the ability to produce pro-inflammatory cytokine in intratumoral T_{reg} cells. Together, our results suggest that CD36 expression specifically supports intratumoral T_{reg} cells suppressive functions.

CD36 deficiency stimulates apoptosis in intratumoral T_{reg} cells

To investigate the underlying basis for the reduced cellularity of CD36-deficient T_{reg} cells in the TME, we first examined proliferative ability by staining Ki67 (Extended Data Fig. 3j) and found that CD36 deficiency did not alter proliferation in intratumoral T_{reg} cells. However, we observed higher amounts of cleaved caspase-3 (Fig. 4a) and Annexin V staining (Extended Data Fig. 3k) in CD36-deficient intratumoral T_{reg} cells. CD36 deficiency did not enhance cleaved caspase-3 abundance in T_{reg} cells from thymus and other secondary lymphoid organs, except a slight increase in draining lymph nodes (Extended Data Fig. 3l), indicating that intratumoral T_{reg} cells require CD36-mediated regulation to prevent apoptosis. Since mitochondrial metabolism and fitness have been suggested to modulate T_{reg} cell suppressive function and survival[22,25,32,33], we then examined whether CD36-deficient intratumoral T_{reg} cells fail to sustain mitochondrial fitness. Strikingly, compared to wild-type T_{reg} cells, CD36-deficient intratumoral T_{reg} cells, but not T_{reg} cells in other tissues, displayed reduced mitochondrial membrane potential as measured by MitoTracker DeepRed staining (Fig. 4b). This observation was further supported by electron microscopy analysis in which we found that intratumoral T_{reg} cells from $T_{reg}^{Cd36-/-}$ mice had fewer mitochondria (Fig. 4c) as well as fewer cristae in each mitochondrion (Fig. 4d). Nevertheless, wild-type and CD36-deficient splenic T_{reg} cells displayed comparable numbers of mitochondria and crista density. By examining the transcriptome of YFP^+ intratumoral T_{reg} cells in both tumor-bearing *Foxp3*$^{YFP\text{-}Cre/+}$*Cd36*$^{fl/fl}$ and *Foxp3*$^{YFP\text{-}Cre/+}$ female mice, we found that CD36-deficient T_{reg} cells (Cre^+ population in *Foxp3*$^{YFP\text{-}Cre/+}$*Cd36*$^{fl/fl}$ mice) in tumors had less expression of mitochondrial genes encoding mitochondrial tRNAs, which control translation of proteins for electron transport chain, compared to wild-type intratumoral T_{reg} cells (Fig. 4e). This result further supports that CD36-deficient intratumoral T_{reg} cells fail to maintain mitochondrial fitness. To further elucidate the impact of CD36 on T_{reg} mitochondrial metabolism, we treated iT_{reg} cells generated from either wild-type or CD36-deficient $CD4^+$ T cells with cancer cell-conditioned medium to induce CD36 expression as shown before. We then performed the Seahorse extracellular flux assays and found that CD36-deficient T_{reg} cells demonstrated reduced oxygen consumption rates (OCR) (Fig. 4f and Extended Data Fig. 4a) but increased glycolytic rates (Extended Data Fig. 4b-c). These results suggest that CD36 ablation can impair oxidative phosphorylation (OXPHOS) and skew the metabolic preference of T_{reg} cells toward aerobic glycolysis. In light of these observations, we speculated that enhanced CD36 expression in intratumoral T_{reg} cells may support T_{reg} metabolic flexibility via modulation of mitochondrial fitness in response to the TME-imposed metabolic stress[28,34,35]. We therefore examined whether CD36-deficient T_{reg} cells displayed survival defects in response to metabolic challenges. In contrast to normal culture conditions (RMPI plus 10% FBS; designated RMPI), CD36-deficient T_{reg} cells exposed to cancer cell-conditioned medium exhibited reduced viability (Extended Data Fig. 4d). Since lactic acid concentrations can be higher in cancer cell-conditioned medium and the accumulation of lactic acid is a common feature of the TME, we thus postulated that CD36-deficient T_{reg} cells might fail to sustain survival in this condition due to

concentrations of lactic acid. In support of this postulate, we found that CD36-deficient T_{reg} cells displayed a profound survival defect in response to increasing concentrations of lactic acid (Fig. 4g). Interestingly, a recent study has suggested that elevated electron transport chain activity results in an increased NAD/NADH ratio to support lactic acid conversion into pyruvate in T_{reg} cells[26], which can support survival of T_{reg} cells in a lactic acid-enriched condition. Thus, we speculated that CD36-deficient T_{reg} cells may have a lower NAD/NADH ratio compared to wild-type T_{reg} cells due to reduced mitochondrial fitness and OXPHOS. Indeed, CD36-deficient T_{reg} cells had a lower NAD/NADH ratio compared to wild-type T_{reg} cells (Fig. 4h), and supplementation with nicotinamide riboside (NR) to replenish NAD[36] partially rescued the viability of CD36-deficient T_{reg} cells exposed to cancer cell-conditioned medium (Fig. 4i). Hence, the failure of CD36-deficient intratumoral T_{reg} cells to persist *in vivo* might result from reduced mitochondrial fitness and OXPHOS, which allow T_{reg} cells to survive in lactic acid-enriched conditions via an NAD-regulated metabolic process.

CD36-PPAR-β signaling orchestrates metabolic adaptation in intratumoral T_{reg} cells

To understand how CD36 stimulates mitochondrial fitness in intratumoral T_{reg} cells, we assessed changes in the transcriptomes of intratumoral and circulating T_{reg} cells from breast cancer patients[29]. As expected, intratumoral T_{reg} cells up-regulated genes controlling mitochondrial functions and biogenesis (Extended Data Fig. 5a). Moreover, we found that intratumoral T_{reg} cells displayed increased expression of genes involved in the PPAR signaling pathway (Fig. 5a). Since CD36 has been suggested to support metabolic flexibility in metabolic tissues by boosting PPAR-β- and PPAR-γ-dependent regulation of mitochondrial activity and biogenesis[37–39], we postulated that CD36-induced metabolic reprogramming might promote mitochondrial fitness in intratumoral T_{reg} cells by providing lipid signals to adjust PPAR transcriptional regulation. To test this, we crossed both *Pparb*$^{fl/fl}$ and *Pparg*$^{fl/fl}$ mice with *Foxp3*$^{YFP\text{-}Cre}$ mice to obtain Treg-specific PPAR-β-deficient mice (designated $T_{reg}^{PPARβ\text{-}/\text{-}}$) and PPAR-γ-deficient mice (designated $T_{reg}^{PPARγ\text{-}/\text{-}}$), respectively. We observed that genetic ablation of PPAR-γ in T_{reg} cells impaired neither accumulation of intratumoral T_{reg} cells nor YUMM1.7 melanoma growth (Extended Data Fig. 5b-d). In contrast, $T_{reg}^{PPARβ\text{-}/\text{-}}$ mice recapitulated the characteristic features of $T_{reg}^{Cd36\text{-}/\text{-}}$ mice, including reduced intratumoral T_{reg} accumulation (Fig. 5b), growth deceleration of engrafted YUMM1.7 melanoma (Fig. 5c,d), and an increase in $CD8^+$ TILs (Extended Data Fig. 5e). Similar to CD36-deficient intratumoral T_{reg} cells, PPAR-β-deficient intratumoral T_{reg} cells displayed reduced mitochondrial membrane potential compared to wild-type intratumoral T_{reg} cells (Fig. 5e). PPAR-β-deficient intratumoral T_{reg} cells expressed less CD36 compared to wild-type intratumoral T_{reg} cells (Extended Data Fig. 5f). We further found that intratumoral T_{reg} cells up-regulated expression of multiple target genes of PPAR-β compared to T_{reg} cells in spleens and draining lymph nodes of tumor-bearing mice (Fig. 5f), suggesting that intratumoral T_{reg} cells might increase PPAR-β activity. To elucidate the relationship between CD36 and PPAR-β activation and their roles on supporting accumulation of intratumoral T_{reg} cells, we speculated that treating PPAR-β selective agonist (GW501516) could bypass the requirement of CD36 to sustain mitochondrial fitness and survival in CD36-deficient intratumoral T_{reg} cells (Fig. 5g). We then treated YUMM1.7 melanoma-engrafted wild-type mice and $T_{reg}^{Cd36\text{-}/\text{-}}$ mice with either GW501516 or control

vehicle for two weeks and found that treatment with GW501516 restored tumor growth as well as intratumoral T_{reg} cell abundance in $T_{reg}^{Cd36-/-}$ mice (Fig. 5h,i). In addition, intratumoral T_{reg} cells from GW501516-treated $T_{reg}^{Cd36-/-}$ mice had increased mitochondrial membrane potentials and less cleaved caspase-3 compared to DMSO- treated $T_{reg}^{Cd36-/-}$ mice (Fig. 5j,k). In parallel, GW501516 treatment in CD36-deficient T_{reg} cells increased NAD/NADH ratios (Extended Data Fig. 5g), indicating that CD36-controlled lipid uptake activates PPAR-β pathways to support mitochondrial fitness and enhancement of NAD/NADH ratios in intratumoral T_{reg} cells. Moreover, the activation of PPAR-β pathways may further amplify CD36-mediated metabolic adaptation in intratumoral T_{reg} cells by enhancing CD36 expression. Altogether, these results reveal that CD36-PPAR-β signaling orchestrate metabolic programs to support T_{reg} persistence in the TME.

CD36-targeting reinforces antitumor immunity by impairing intratumoral T_{reg} cells

Next, we hypothesized that blocking CD36-mediated metabolic adaptation could specifically disturb intratumoral T_{reg} cells without systemic loss of T_{reg} cells and global impairment of T_{reg} suppressive functions. To test this, we treated Yumm1.7 melanoma-engrafted mice with an anti-CD36 monoclonal antibody (mAb), which interferes with CD36-mediated fatty acid and oxidized low-density lipoprotein uptake[40]. We found that anti-CD36 mAb treatment reduced tumor growth (Fig. 6a) and was accompanied by reduced accumulation of intratumoral T_{reg} cells, while the T_{reg} cell population was sustained in spleen and draining lymph nodes (Fig. 6b and Extended Data Fig. 6a). Similar to genetic ablation of *Cd36* in T_{reg} cells, anti-CD36 mAb treatment promoted apoptosis in intratumoral T_{reg} cells (Fig. 6c), and led to a significant increase in tumor infiltration of $CD8^+$ T cells (Extended Data Fig. 6b). In addition, treating mice with an anti-CD36 mAb improved the production of anti-tumor effector cytokines in $CD8^+$ and $CD4^+$ TILs (Extended Data Fig. 6c-d). Since CD36 expression can support metabolic flexibility and metastasis in cancer cells as well as other immune cells[40,41], the anti-tumor responses induced by anti-CD36 mAb may be T_{reg} cell-independent. To this end, we performed the same treatment using $T_{reg}^{Cd36-/-}$ mice as recipients. Our results showed that anti-CD36 mAb treatment was incapable of suppressing tumor progression in $T_{reg}^{Cd36-/-}$ mice (Fig. 6d), indicating that the anti-tumor responses induced by anti-CD36 mAb treatment might mainly result from targeting CD36 expressed in T_{reg} cells instead of other CD36-expressing cells.

As T cell exhaustion may limit the therapeutic outcomes of T_{reg} cell-targeting interventions[31], we postulated that reinvigorating exhausted T cells with PD-1 blockade may potentiate the anti-tumor effects of CD36 blockade to restrain tumor progression. Indeed, we found that anti-PD-1 mAb more effectively limited tumor progression and prolonged survival in tumor-bearing $T_{reg}^{Cd36-/-}$ mice compared to wild-type mice (Fig. 6e,f). In addition to genetic ablation of CD36 in T_{reg} cells, we observed that anti-PD-1 mAb also potentiated the anti-tumor responses of anti-CD36 mAb in both the genetically engineered Braf/PTEN melanoma mouse model (Fig. 6g) and the YUMM1.7 engraftment model (Extended Data Fig. 6e,f). These results demonstrate that targeting CD36 in T_{reg} cells might reprogram the TME towards more immunostimulatory conditions, which may therapeutically complement the effect of PD-1 blockade to counteract T-cell exhaustion.

This points to CD36 blockade as a new potential immunotherapeutic intervention with reduced side effects caused by systemic impairment of T_{reg} cells.

Discussion

Exploiting the regulatory circuits by which metabolic processes orchestrate immune responses in immune cells is an attractive strategy for fine-tuning host immunity in diseases. Here we uncover that CD36-PPAR-β signaling sustains survival and functional fitness in intratumoral T_{reg} cells by modulating mitochondrial fitness and NAD levels. Owing to the uniqueness of the metabolic stress occurring in the TME and the selectivity of CD36-PPAR-β signaling for intratumoral T_{reg} cells, targeting CD36 may provide broad therapeutic potential with limited negative impact on immune and peripheral tissue homeostasis in cancer patients. Moreover, the additive anti-tumor effects elicited by combined treatment with PD-1 blockade and CD36 targeting further warrant the development of CD36 inhibition approaches as potential cancer treatments.

Although our results reveal that CD36-mediated metabolic adaptation, including mitochondrial fitness and NAD production, support intratumoral T_{reg} survival and suppressive functions, it remains unknown whether the suppressive functions of intratumoral T_{reg} cells are modulated by lipid-derived signals or the enhanced usage of lactic acids. While OXPHOS is thought to promote T_{reg} immunosuppression via undefined mechanisms[42], it remains unexplored whether distinct fuels driving OXPHOS may differentially impact suppressive activity of T_{reg} cells. Given that T_{reg} cells could convert lactic acid into pyruvate that might be further utilized for production of acetyl-CoA, α-ketoglutartae, succinate and fumurate, which can be used for modulating transcriptome and function in immune cells via epigenetic regulations[43,44], it is possible that CD36-mediated metabolic adaptation could instruct intratumoral T_{reg}-specific transcriptome that support unique suppressive activities. On the other hand, aerobic glycolysis has also been suggested to support expansion of intratumoral T_{reg} cells[45]. Since accumulation of NADH can impede glycolytic activity, it is also possible that the declined mitochondrial fitness in CD36-deficient intratumoral T_{reg} cells could hamper expansion and survival by restricting glycolysis. Of note, in this study, the authors report that intratumoral T_{reg} cells increased lipid content as a result of elevated glycolysis that supports fatty acid synthesis and cell expansion[45]. In contrast to our conclusion that intratumoral T_{reg} cells increase lipid uptake, the author does not observe increased lipid uptake in intratumoral T_{reg} cells by using systemic injection of Bodipy-conjugated lipids into tumor-bearing mice. We reason that the injection of limited amounts of Bodipy-conjugated lipids may not be sensitive enough to detect enhanced lipid uptake ability in intratumoral T_{reg} cells. However, in agreement with our observation, both studies suggest that intratumoral T_{reg} cells engage distinct metabolic processes that could be used to fuel survival and suppressive activity. Thus, elucidation of the mechanistic link between metabolic adaptation and specialized transcriptome dictating suppressive activity and tumor-specific behavior in intratumoral T_{reg} cells is therefore an important avenue for future research. A better understanding of these questions may allow us to incorporate interventions targeting lactic acid production in cancer cells and lactic acid uptake in T_{reg} cells for cancer treatment.

Europe PMC Funders Author Manuscripts

Although T_{reg}-specific ablation of CD36 or PPAR-β does not compromise formation of T_{reg} cells in thymus and secondary lymphoid organs, it remains likely that the induction of CD36-PPAR-β signal in particular circumstance, such as tumor, might synergize with FoxP3-mediated metabolic program to boost mitochondrial activity and oxidative phosphorylation in T_{reg} cells. The robust increase of OXPHOS in this circumstance may further support DNA methylation-mediated chromatin remodeling that is critical for the expression of FoxP3 target genes via generation of metabolites controlling DNA demethylase activity. Furthermore, as exposure of cancer cell-conditioned medium stimulates expression of CD36 in T_{reg} cells, while PPAR-β-deficient intratumoral T_{reg} cells express lower levels of CD36, it is likely that lipids produced by tumor cells serve as immunosuppressive regulators to support the engagement of CD36-dependent metabolic adaptation in intratumoral T_{reg} cells. Future studies elucidating the identity of these lipids can shed light on the impact of tumor metabolism on the TME.

Methods

Mice

C57BL/6/J, *Foxp3*$^{YFP\text{-}Cre}$, *Rag1*$^{-/-}$ (B6.129S7-Rag1^{tm1Mom}/J) mice were purchased from Jackson Laboratories. *Cd36*$^{fl/fl}$ mice were generated as previously described[46] and provided by I. J. Goldberg at New York University. *Pparg*$^{fl/fl}$ and *Pparb*$^{fl/fl}$ mice were generated and provided by B. Desvergne at University of Lausanne[47]. BRafCA; Tyr::CreER; Ptenlox4-5 (Braf/Pten) was obtained from M. Bonsenburg at Yale University. *K-ras*$^{LSL\text{-}G12D/+}$/*p53*$^{fl/fl}$ conditional mouse model of NSCLC was obtained from E. Meylan at Ecole Polytechnique Fédérale de Lausanne. Animals were housed in specific-pathogen-free facilities at the University of Lausanne and all experimental studies were approved and performed in accordance with guidelines and regulations implemented by the Swiss Animal Welfare Ordinance.

Cell lines and in vitro cultures

YUMM1.7 melanoma cell line was kindly provided by M.Bosenberg[48]. YUMM1.7 and B16-ova melanoma cell lines were cultured in DMEM with 10% fetal bovine serum and 1% penicillin-streptomycin and used for experiments when in exponential growth phase. MC38 colon adenocarcinoma cell line was provided by M. De Palma at Ecole Polytechnique Fédérale de Lausanne and was maintained in IMDM with 10% fetal bovine serum and 1% penicillin-streptomycin.

Cancer cell-conditioned medium and iT_{reg} cell culture

iT_{reg} cells were generated by activating naïve $CD4^+$ T cells with Dynabeads conjugated with anti-CD3 and anti-CD28 mAbs (ThermoFisher) in RMPI media supplemented with 10% FBS, 10 ng/ml TGF-β and 50U/ml IL-2 for three days. Then activated $CD4^+$ T cells were maintained in RPMI media plus 10% FBS and 50 U/ml IL-2 for another 2 days. Differentiated iT_{reg} cells were firstly sorted by using FACS cell sorter and then incubated in indicated culture condition for 48 h. The survival and NAD/NADH levels of iT_{reg} cells were then determined by live/dead staining and ELISA kits, respectively. For NAD/NADH measurement in CD36-deficient iT_{reg} cells treated with PPAR-β agonist, sorted iT_{reg} cells

were cultured in cancer cell-conditioned medium in the presence of DMSO or GW50156 for 48 h. Control RPMI for iT_{reg} cell in vitro treatment was prepared with RPMI 1640 medium (Biological Industries) supplementing with 2 mM Glucose, 10 mM Glutamine, 10% dialyzed FBS, 0.1% β-mercaptoethanol, and indicated concentrations of lactic acids. YUMM1.7 cancer cell-conditioned medium was collected by incubating YUMM1.7 cells (70-80% density) with control RPMI described above for 18 h. Then, culture medium was collected and centrifuged at 2000 rpm for 15 min to remove debris and cancer cells as cancer cell-conditioned medium. YUMM1.7 cancer cell-conditioned medium collected as described above was treated with Cleanascite™ reagent (Biotech Support Group) prior to T_{reg} cell culture at a volume ratio of 1:5 according to the manufacturer's instruction.

Ex vivo suppression assay

$CD8^+$ T cells from spleen of Ly5.1 mice were enriched using negative selection kit (MojoSort Mouse CD8 T cell isolation kit, BioLegend), and stained with CellTrace™ CFSE cell proliferation kit (ThermoFisher) for 15 min at 37 °C. 1×10^4 $CD8^+$ cells were seeded into 96-well round plate in RPMI medium consisting of 50 U/ml IL-2. $CD44^+YFP^+$ T_{reg} cells ($CD45.2^+$) isolated from splenocytes or TILs of *FoxP3*$^{YFP\text{-}Cre}$ or $T_{reg}^{CD36\text{-}/\text{-}}$ mice were added according to indicated ratios for T_{reg}:T_{eff}. Then, anti-CD3–CD28-conjugated Dynabeads (ThermoFisher) were supplemented into cultures except for negative control groups. Cells were incubated at 37 °C, 5% CO_2 for 72 h and then the proliferation of $CD8^+$ T cells were determined by CFSE dilution with flow cytometry analysis.

Tumor engraftment and treatment of tumor-bearing mice

For tumor induction, 3-week-old Braf/Pten mice were treated with 4-hydroxytamoxifen on the skin surface as described before to induce tumor formation[49]. For tumor engraftment, 5×10^4 cells YUMM1.7, B16-OVA, or one million1×10^6 MC38 tumor cells were injected subcutaneously in 50 μl PBS. Tumors were measured every 2-3 days post tumor engraftment or indicated treatments and calculated. Tumor volume was calculated by volume = (length × width^2)/2 for engrafted tumor or volume = (length × width × height) for inducible tumor. For in vivo treatment, Yumm1.7-bearing mice were administrated every 3 days with either DMSO or PPAR-β agonist (GW 501516) (1 mg per kg of body weight, Cayman Chemical) by intraperitoneal injection. For antibody-based treatment, tumor-bearing mice were treated with anti-PD-1 antibody (200 μg per injection, BioXcell, clone 29F.1A12) and anti-CD36 antibody (200 μg per injection, clone CRF D-2712 [50], provided by R. Silverstein at Medical College of Wisconsin) according to indicated combination by intraperitoneal injection. For antibody treatment in the Braf/Pten mouse model, four weeks after tumor induction, tumor-bearing Braf/Pten mice were treated with anti-CD36 antibody and/or anti-PD-1 antibody as indicated above for a period of 10 days. All experiments were conducted according to Swiss federal regulations.

Tumor digestion and cell isolation

Tumors were minced into small pieces in RPMI containing 2% FBS, 1% penicillin-streptomycin (p/s), DNase I (1 μg/ml, Sigma-Aldrich), and collagenase (0.5 mg/ml, Sigma-Aldrich) and kept for digestion for 40 min at 37 °C, followed by the filtration with a 70 μm cell strainer. Filtered cells were incubated with ACK lysis buffer (Invitrogen) to lyse red

blood cells and then washed with fluorescent activated cell sorter (FACS) buffer (phosphate-buffered saline with 2% fetal bovine serum and 2 mM EDTA). Tumor-infiltrating leukocytes were further enriched by percoll density gradient centrifugation (800x*g*, 30 min) at room temperature as described before[51].

Flow cytometry, cell sorting and antibodies

Single cell suspensions were incubated with Fc receptor-blocking anti-CD16/32 (93) and anti-CD351 (TX61) antibodies (BioLegend) on ice for 10 min before staining. Cell suspensions were first stained with LIVE/DEAD® Fixable Violet Dead Cell Stain Kit (ThermoFisher) at 37 °C for 10 min. Aftrer washing, surface proteins were stained for 30 min at 4 °C. To detect cytokine production upon *ex-vivo* re-stimulation, cell suspensions were re-suspended in RPMI 1640 with 10% FBS and then added to plates coated with 1 μg/ml anti-CD3 antibody (clone 145-2C11, BioLegend) and anti-CD28 antibody (clone 37.51, BioLegend) for another 5 h at 37 °C in the presence 2.5 μg/ml Brefeldin A Solution (BFA) (BioLegend). Cells were processed for surface marker staining as described above and then intracellular cytokine staining. Samples were analyzed on LSRII flow cytometers (BD Biosciences) and data were analyzed with FlowJo. Cells were sorted either on FACSAria™ III sorter (BD Biosciences) or SH800S Cell Sorter (Sony). Human T_{reg} cells were defined by the following staining: Live/Dead-neg/CD45RA-neg/CD3-pos/CD4-pos/CD8-neg/CD25-pos/FoxP3-pos; Mouse non T_{reg} CD4 T cells were defined by the following staining: CD45-pos/CD3-pos/CD4-pos/CD8-neg/FoxP3-neg; CD8 T cells were defined by the following staining: CD45-pos/CD3-pos/CD8-pos/CD4-neg; T_{reg} cells were defined by the following staining: CD45-pos/CD3-pos/CD4-pos/CD8-neg/FoxP3-pos. The following antibodies against mouse proteins were used: anti-CD45 (30-F11), anti-CD3ε (17A2), anti-CD4 (RM4-5), anti-CD8α (53.6.7), anti-CD44 (IM7), anti-62L (Mel-14), anti-PD1 (RMP1-30), anti-CD134 (OX40) (OX-86), anti-CD357 (GITR) (DTA-1), anti-CD36 (CRF D-2712), anti-IgA (mA-6E1), anti-FoxP3 (MF-14), anti-GFP/YFP (FM264G), anti-IFN-γ (XMG1.2), anti-TNF (MP6-XT22), anti-IL-17A (TC11-18H10.1), anti-Ki67 (16A8), anti-CD278 (ICOS) (15F9), anti-CD152 (CTLA4) (UC10-4B9), cleaved Caspase-3 (Asp175). The following antibodies against human proteins were used: Anti-CD45 (2D1), anti-CD3 (SK7), anti-CD4 (SK3), anti-CD25 (BC96), anti-CD8 (RPA-TP), anti-CD36 (TR9), anti-PD1 (E12.1), anti-GITR (eBIOAITR), and anti-FoxP3 (150D). These antibodies were purchased from BioLegend, eBiosciences and Cell Signaling.

Mitochondrion, fatty acid uptake and lipid content assay

For measuring mitochondrial membrane potential, cells were washed and incubated with pre-warmed (37 °C) staining solution (RPMI with 2% FBS) containing MitoTracker® Deep Red FM (ThermoFisher) and MitoTracker® Green FM (ThermoFisher) at the working concentrations of 10nm and 100nM for 15min, respectively. After staining, the cells were washed and resuspended in fresh FACS buffer for surface marker staining as described above. For measuring fatty acid uptake, cells were incubated in RPMI medium (or human T cell culture medium) containing C1-BODIPY® 500/510 C12 (Life Technologies) at final concentration of 0.5 μM for 15 min at 37 °C. After incubation, cells were washed with FACS buffer for surface staining. For lipid content detection, after permeablization and fixation,

cells were stained using BODIPY® 493/503 (Life Technologies) at a final concentration of 500 ng/ml together with other intracellular proteins.

RNA sequencing and bioinformatics analysis

500-600 viable $CD4^+CD44^+YFP^+$ intratumoral T_{reg} cells from heterozygous *Foxp3*$^{YFP\text{-}Cre/+}$ female mice or heterozygous *Foxp3*$^{YFP\text{-}Cre/+}$*Cd36*$^{fl/fl}$ female mice were isolated by FACS cell sorters (with at least 99% purity) directly into 4 μl lysis buffer consisting of 0.2 % (vol/vol) Triton X-100 solution (MgBCH-Axon Lab) and RNase inhibitor (Clontech). Plate containing samples were sealed, flash-frozen and kept at −80 °C before further processing following a version of the Smart-Seq2 protocol described before[52]. The RNA-sequencing raw data were processed through the standard RNA-seq analysis pipeline. Briefly, read alignment was examined using tophat2 v2.1.0 and then compared to the Mus musculus GRCm38.p4 genome version. Following the alignment, reads mapped to each gene were annotated using HTseq count. The differential expression analyses were conducted based on the DESeq2 R library. The differential expression test and visualization were then examined by the START Web-based RNA-seq analysis resources[53]. Gene Set Enrichment Analysis (GSEA) was performed using GSEA software.

Electron microscopy analysis and histology analysis

For electron microscopy analysis, sorted cells were fixed in glutaraldehyde 2.5% (EMS) and osmium tetroxide 1% (EMS) overnight at 4 °C, followed by several washes with water and acetone (Sigma), and embedded in Epon (Sigma) resin the following day. Before imaging, 50 nm slides were prepared by using a Leica Ultracut microtome, and were contrasted using uranyl acetate (Sigma) and Reynolds lead citrate (Sigma). Electron microscope images were taken with a transmission electron microscope Philips CM100 at an acceleration of 80kV with a TVIPS TemCam-F416 digital camera with a magnification of 4800x and 11’000x. Image analysis and quantification were carried out using EMMENU, 3dmod (University of Colorado) and Fifi (ImageJ) software. To quantify mitochondria per sorted cell, a grid was applied and each intersection was defined as being part of the nucleus, cytoplasm or mitochondria and the length of each crista was measured divided by the mitochondrial area for determination of the crista density. For histology analysis, organs were trimmed and placed in the labeled cassettes and fixed in formalin for 24h for further embedding in molten paraffin wax. Paraffin sections at a thickness of 3-5 μm was stained with hematoxylin and eosin according to standard procedures. Images were taken and exported on a Nikon Eclipse Ti-S inverted microscope.

Human patient assessment

This study was performed in accordance with the guidelines of ethic regulation for human samples under approved protocol at Lausanne University Hospital (protocol 87/06), University Hospital Basel (EK128/13) and Memorial Sloan Kettering Cancer Center (00-144 and 19-101). Human samples were analyzed following safety regulation and stained with antibodies for FACS analysis as described above.

T cell transfer model of colitis

Wild-type and CD36-deficient T_{reg} cells were sorted from the spleens of either *Foxp3*$^{YFP\text{-}Cre}$ mice or $T_{reg}^{CD36\text{-}/\text{-}}$ mice and naïve $CD4^+$ T cells were harvested using a combination of negative magnetic selection (MojoSort Mouse CD4 T cell isolation kit, BioLegend) and FACS sorting (>98% purity). To induce colitis, naïve $CD4^+$ cells (5×10^5 cells) were transferred intravenously into *Rag1*$^{-/-}$ recipients. In some recipients, 4×10^5 $CD44^+YFP^+$ T_{reg} cells isolated from splenocytes of *Foxp3*$^{YFP\text{-}Cre}$ mice or $T_{reg}^{CD36\text{-}/\text{-}}$ mice were co-transferred with naïve $CD4^+$ T cells. Recipient mice were monitored and weighted every two or three days after transferring for signs of diseases such as weight loss. Diseases onset usually occurs at 4-5 weeks post-transfer. The endpoints of this study included the determination of body weight loss, colitis length, and diarrhea. In addition, colons and small intestines were collected and processed for further evaluation by Hemotoxylin and Eosin staining.

NAD and NADH measurement

The ratio of nicotinamide adenine dinucleotide (NAD) and nicotinamide adenine dinucleotide hydrate (NADH) were measured by using the commercial NAD/NADH Quantification Kit (Sigma-Aldrich MAK037). The cells were first de-proteinized to prevent the NAD and NADH consumption by enzymes. After washing with cold PBS, cell pellets suspended in NADH/NAD extraction buffer (200 μl) were treated with two repetitive freeze-thaw cycles and then spun at 13,000×g for 5 min at 4 °C. The supernatant was then divided into two aliquots, one was for NAD_{total} detection, and the other one was heated at 60° C for 30 min for NAD decomposition. The samples were then transferred to a 96-well plate for measuring the absorbance of 450 nm. The amount of oxidized NAD (NAD^+) was presented subtracting NADH from NAD_{total}. The ratio of NAD/NADH in a sample could be determined by the following equation: ratio = (NAD_{total} – NADH)/NADH.

Seahorse extracellular flux analyses

Extracellular flux analysis was performed with an XF96 Seahorse Extracellular Flux Analyzer as described before[54] with minor modifications. Cells were treated with oligomycin (0.5 μM, Sigma-Aldrich), FCCP (2 μM, Sigma-Aldrich), rotenone (0.5 μM, Sigma-Aldrich), antimycin A (0.5 μM, Sigma-Aldrich), glucose (10 mM, Sigma-Aldrich) and 2-DG (50 mM, Sigma-Aldrich). Each condition was performed with 3–6 replicates in each single experiment.

Statistical analyses

Statistical analyses were performed using the two-tailed, unpaired, Student's *t*-test. Log-rank (Mantel–Cox) test was used for survival curve analysis. Each point represented a biological replicate and all data were presented as the mean ± SD, or mean ± SEM as indicated. The *P* values were represented as follows: ***$P < 0.001$, **$P < 0.01$ and *$P < 0.05$. $P < 0.05$ was considered statistically significant.

Extended Data

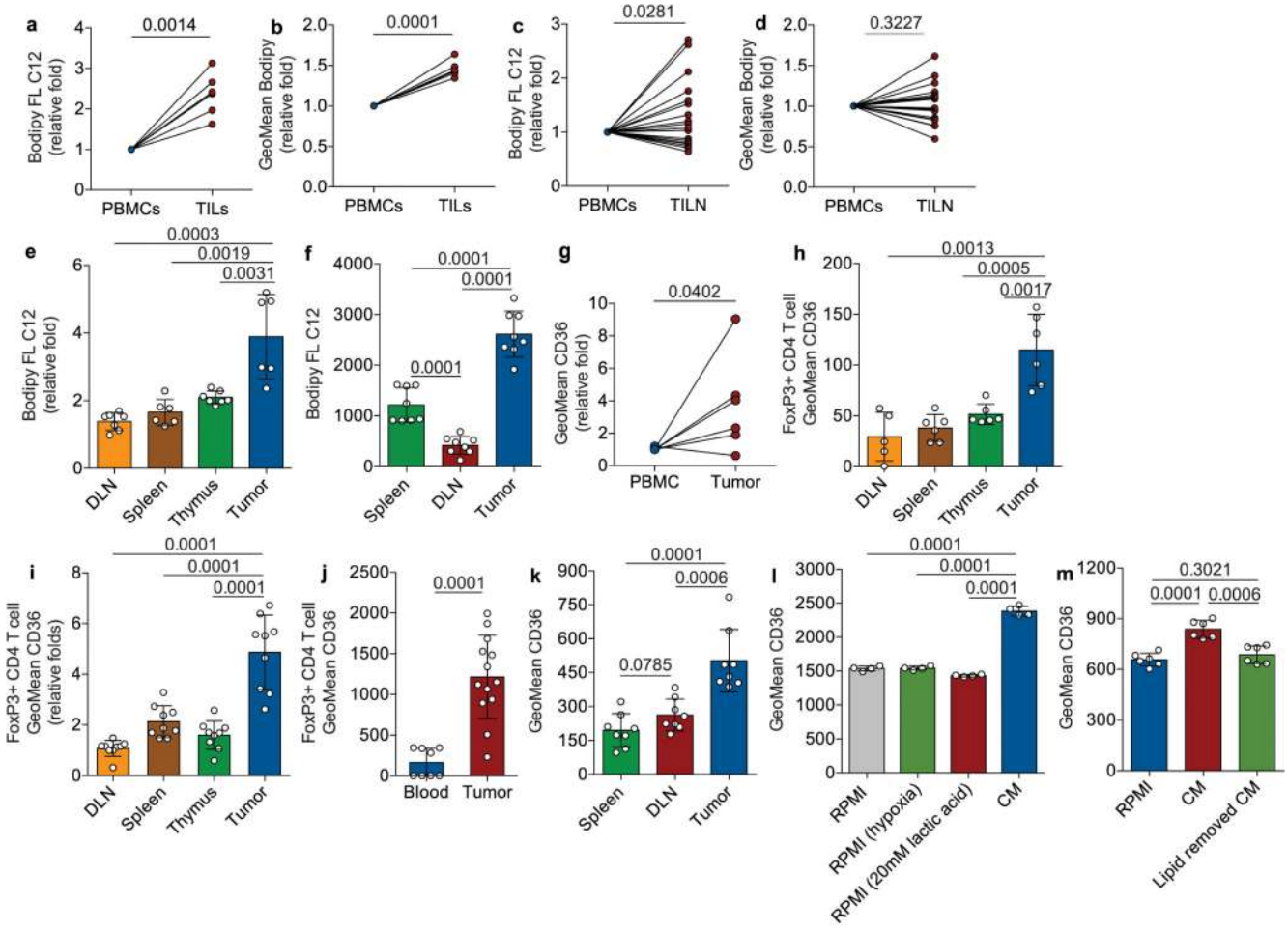

Extended Data Fig. 1. Lipid accumulation and increased CD36 expression in intratumoral T_{reg} cells.

a, b, Quantitative results of geometric mean (GeoMean) fluorescent intensity of Bodipy FL C12 (**a**) and Bodipy 493/503 (Bodipy) (**b**) in T_{reg} cells from paired TILs and PBMCs of non-small cell lung cancer (NSCLC) patients (n=6 per group). **c, d,** Quantitative results of GeoMean fluorescent intensity of Bodipy FL C12 (**c**) and Bodipy 493/503 (**d**) in T_{reg} cells from paired PBMC and tumor infiltrated lymph nodes (TILNs) of melanoma patients (n=19). **e, f,** Quantitative results of fluorescent intensity of Bodipy FL C12 in T_{reg} cells from indicated tissues of B16 melanoma-bearing mice (dLN, n=7; Spleen, n=6; Thymus, n=7; Tumor, n=6) (**e**), and MC38 colon carcinoma-bearing mice (n=8) (**f**). **g,** Quantitative result of GeoMean fluorescent intensity of CD36 surface staining in T_{reg} cells from paired TILs and PBMCs of NSCLC patients (n=6) **h, i, j, k,** Quantitative results of surface expression of CD36 in T_{reg} cells of indicated tissues from B16-OVA melanoma-bearing B6 mice (n=6, one outlier was removed from dLN) (**h**), inducible Braf/Pten melanoma-bearing mice (n=9) (**i**), *K-ras*$^{LSL\text{-}G12D/+}$/*p53*$^{fl/fl}$ mouse model of NSCLC (Blood, n=8; Tumor, n=13) (**j**), and MC38 colon cancer (n=8) (**k**). **l,** CD36 expression in iT_{reg} cells cultured in different indicated conditions for 48h. (RPMI: normal cell culture RPMI 1640 medium indicated in methods; CM, cancer cell conditioned medium, n=4 per group). **m,** CD36 expression in iT_{reg} cells

Europe PMC Funders Author Manuscripts

cultured in cancer cell-conditioned medium treated with control procedure or lipid removal procedure for 48h. (n=6 per group). Data are representative result of at least two independent experiments with similar results (**l, m**) or cumulative results from at least two independent experiments (**a, b, c, d, e, f, g, h, i, j, k**). Each symbol represents one individual. Data are mean ± S.D. and were analyzed by two-tailed, unpaired Student's *t*-test (**e, f, h, i, j, k, l, m**) or two-tailed, paired Student's *t*-test (**a, b**) or one-tailed, paired Student's *t*-test (**c, d, g**).

Europe PMC Funders Author Manuscripts

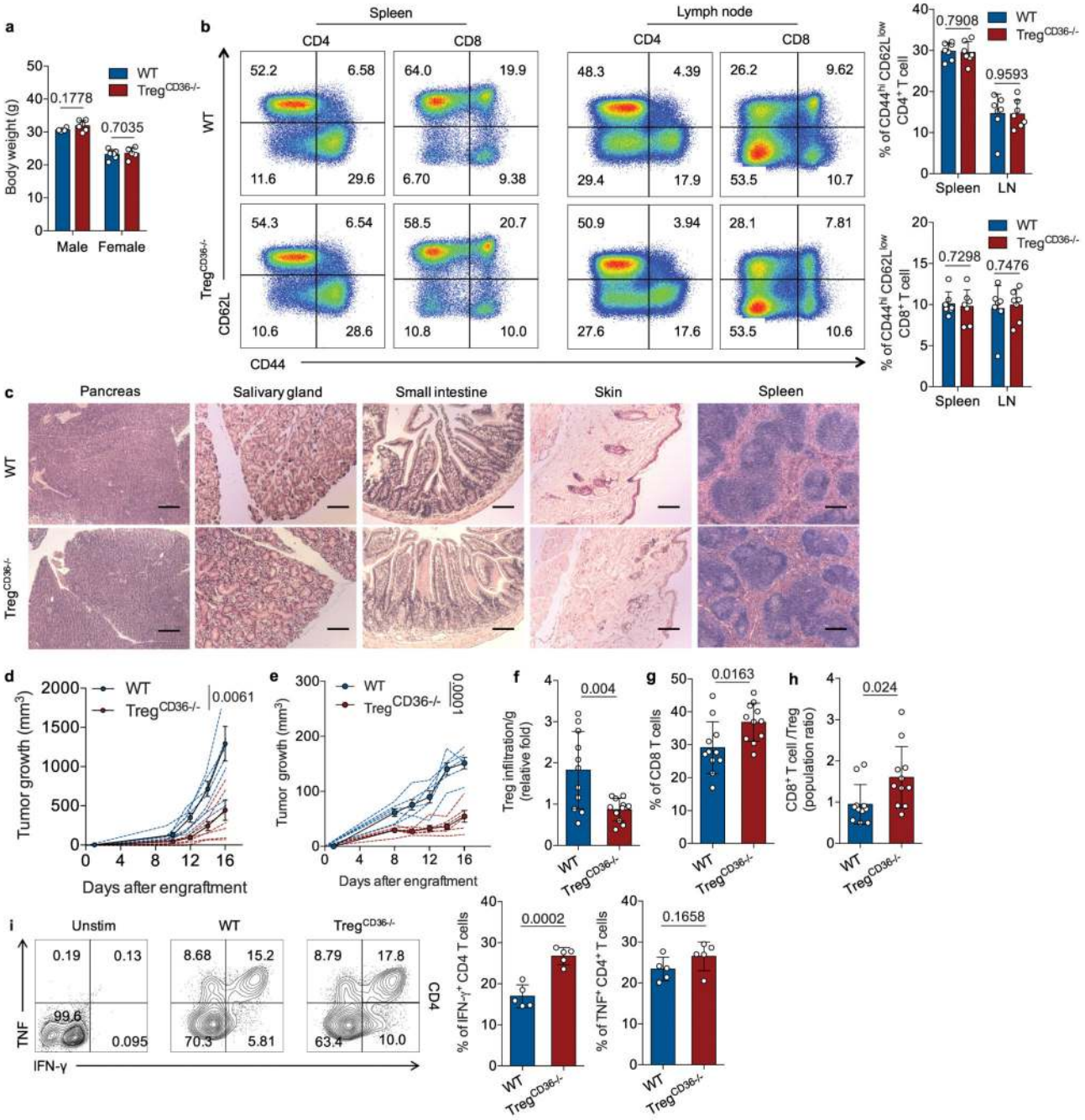

Extended Data Fig. 2. CD36 expression supports the accumulation and suppressive function of intratumoral T_{reg} cells.

a, Body weight of WT and $T_{reg}^{Cd36-/-}$ mice at the age of 21-23 weeks (WT male, n=4; $T_{reg}^{Cd36-/-}$ male, n=6; WT female, n=6; $T_{reg}^{Cd36-/-}$ female, n=5;). **b,** Representative plots (left) and quantitative frequency of $CD44^{hi}/CD62L^{low}$ $CD4^+$ or $CD8^+$ T cells (right) in aged WT and $T_{reg}^{Cd36-/-}$ mice (n=7 per group). **c,** Representative images of hematoxylin and eosin (H&E) staining for indicated tissues from WT or $T_{reg}^{Cd36-/-}$ mice at the age of 21-23 weeks. Scale bar, 200 μm. **d, e,** Tumor growth of B16-OVA melanoma (n=7 per group) (**d**)

Europe PMC Funders Author Manuscripts

or MC38 colon carcinoma (n=6 per group) (**e**) from WT or $T_{reg}^{Cd36-/-}$ mice. **f, g, h,** Absolute number of FoxP3$^+$ T_{reg} cells per gram tumor (**f**), percentage of CD8$^+$ T cells out of CD3$^+$ T cells among tumor-infiltrating T cells (**g**), and the ratio of CD8$^+$ to T_{reg} cell TIL density (**h**) of YUMM1.7 melanoma-bearing WT and $T_{reg}^{Cd36-/-}$ mice (n=11 per group). **i,** Representative plots (left) and percentage of indicated cytokine-producing CD4$^+$ T cells among total tumor-infiltrating CD4$^+$ T cells from indicated mice (right) (n=5 per group). Data are representative result of at least two independent experiments with similar results (**c, d, e, i**) or cumulative results from at least two independent experiments (**a, b, f, g, h)** Each symbol represents one individual. Data are mean ± S.D. (**a, b, f, g, h, i)** or ± S.E.M. (**d, e**) and were analyzed by two-tailed, unpaired Student's *t*-test.

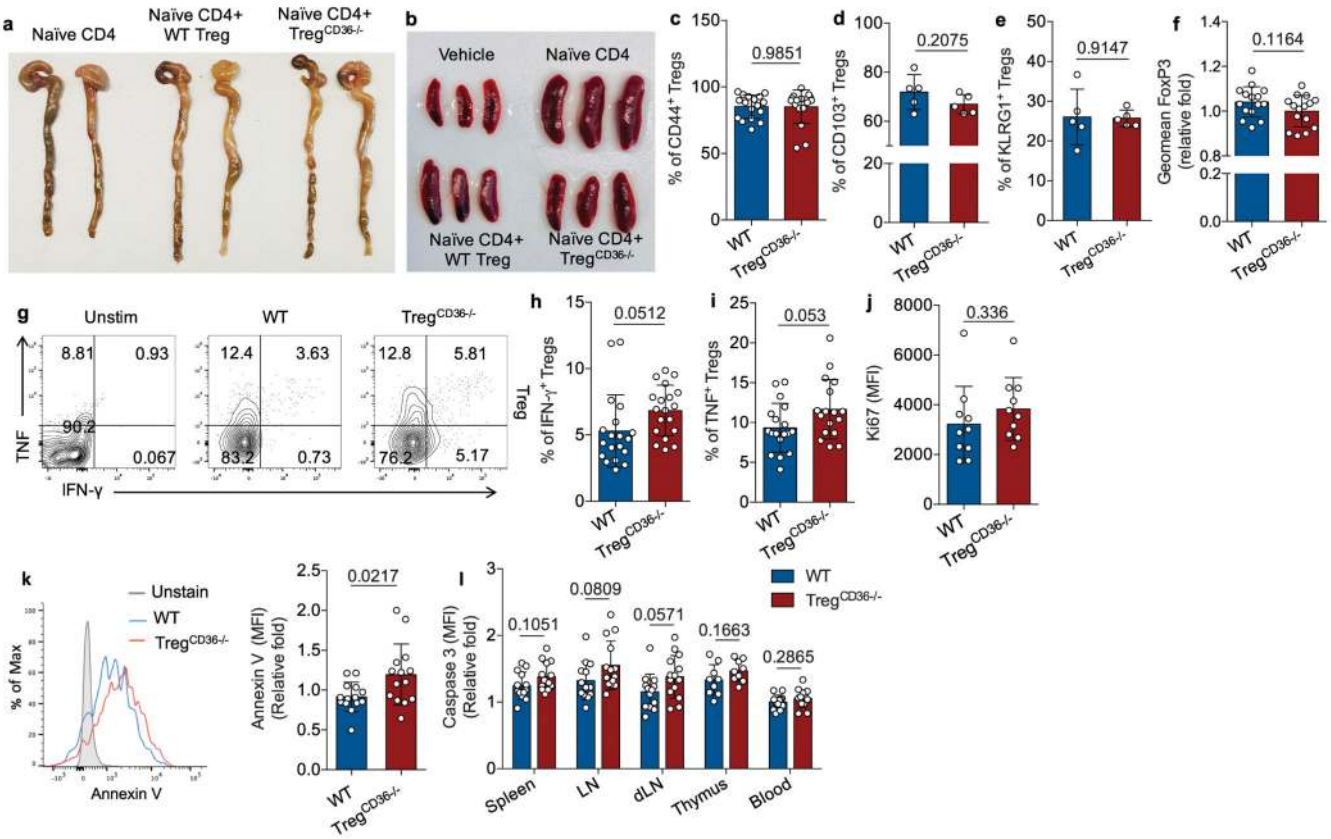

Extended Data Fig. 3. Effects of CD36 in expression of activation markers and stability of intratumoral T_{reg} cells.

a, Representative images of guts (**a**) and spleens (**b**) from indicated group of $Rag1^{-/-}$ mice. **c, d, e,** Expression of CD44 (n=17) (**c**), CD103 (n=5) (**d**), and KLRG1 (n=5) (**e**) in intratumoral T_{reg} cells of YUMM1.7 melanoma-bearing WT and $T_{reg}^{Cd36-/-}$ mice. **f,** The expression of YFP in intratumoral T_{reg} cells of YUMM1.7 melanoma-bearing WT and $T_{reg}^{Cd36-/-}$ mice (n=15). **g, h, i,** Representative plots of IFNγ and TNF production among total intratumoral T_{reg} cells from indicated mice (**g**), and quantitative result of percentage of IFNγ-producing (n=19 per group) (**h**) and TNF-producing (n=18, one outlier was removed from T_{reg}*Cd36-/-*) (**i**) T_{reg} cells among total intratumoral T_{reg} cells of indicated mice. **j,** Expression of Ki67 in intratumoral T_{reg} cells of YUMM1.7 melanoma-bearing WT and $T_{reg}^{Cd36-/-}$ mice (n=10 per group). **k,** Representative histograms (left) and quantitative analysis (right) of Annexin V staining in intratumoral T_{reg} cells from WT and $T_{reg}^{Cd36-/-}$ tumor-bearing mice (n=14 per group). **l,** Quantitative analysis of cleaved caspase-3 levels in T_{reg} cells of indicated tissues from WT (n=13 per group except for thymus, n=9) and $T_{reg}^{Cd36-/-}$ (n=14 per group except for thymus, n=9) tumor-bearing mice. LN: non-draining lymph node; DLN: draining lymph node. Data are representative results of two independent experiments with similar results (**a, b, d, e**) or cumulative results from at least three independent experiments (**c, f, g, h, i, j, k, l**). Each symbol represents one individual. Data are mean ± S.D. (**c, d, e, f, h, i, j, k, l**) and were analyzed by two-tailed, unpaired Student's *t*-test.

Europe PMC Funders Author Manuscripts

Europe PMC Funders Author Manuscripts

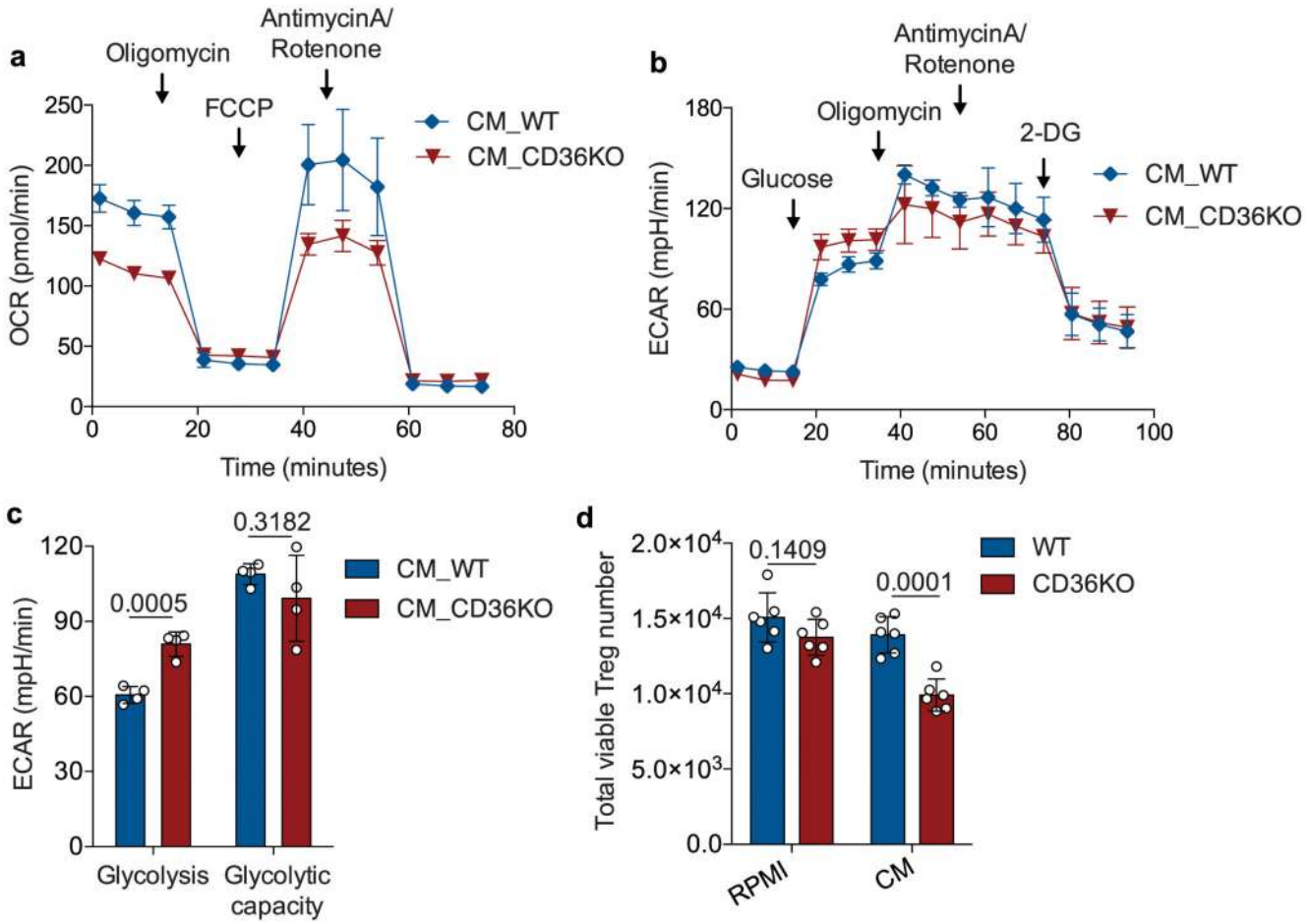

Extended Data Fig. 4. CD36-deficiency results in a metabolic shift and elevated apoptosis in T_{reg} cells.

a, Indicated iT_{reg} cells cultured in cancer cell-conditioned medium for 48 hrs (n=3 per group). Oxygen consumption rate (OCR) of indicated iT_{reg} cells was measured and then followed by treatment with oligomycin, FCCP, and antimycin A plus Rotenone (n ≥4 per group). **b,** Indicated iT_{reg} cells cultured in cancer cell-conditioned medium for 48 hrs (n ≥4 per group) and then media were refreshed with Seahorse Flux assay media without glucose. Basel extracellular acidification rate (ECAR) of indicated iT_{reg} cells was measured and then followed by treatment with glucose, oligomycin, FCCP and 2-DG (n=4 per group). **c,** Quantitative result of glycolysis and glycolytic capacity based on the measurement of **b**. **d,** The viability of either WT or $T_{reg}^{Cd36-/-}$ iT_{reg} cells cultured under indicated conditions for 72 hrs (n=6 per group). Data are representative results of three independent experiments with similar results (**a, b, c, d**). Data are mean ± S.D. and were analyzed by two-tailed, unpaired Student's *t*-test (**c, d**).

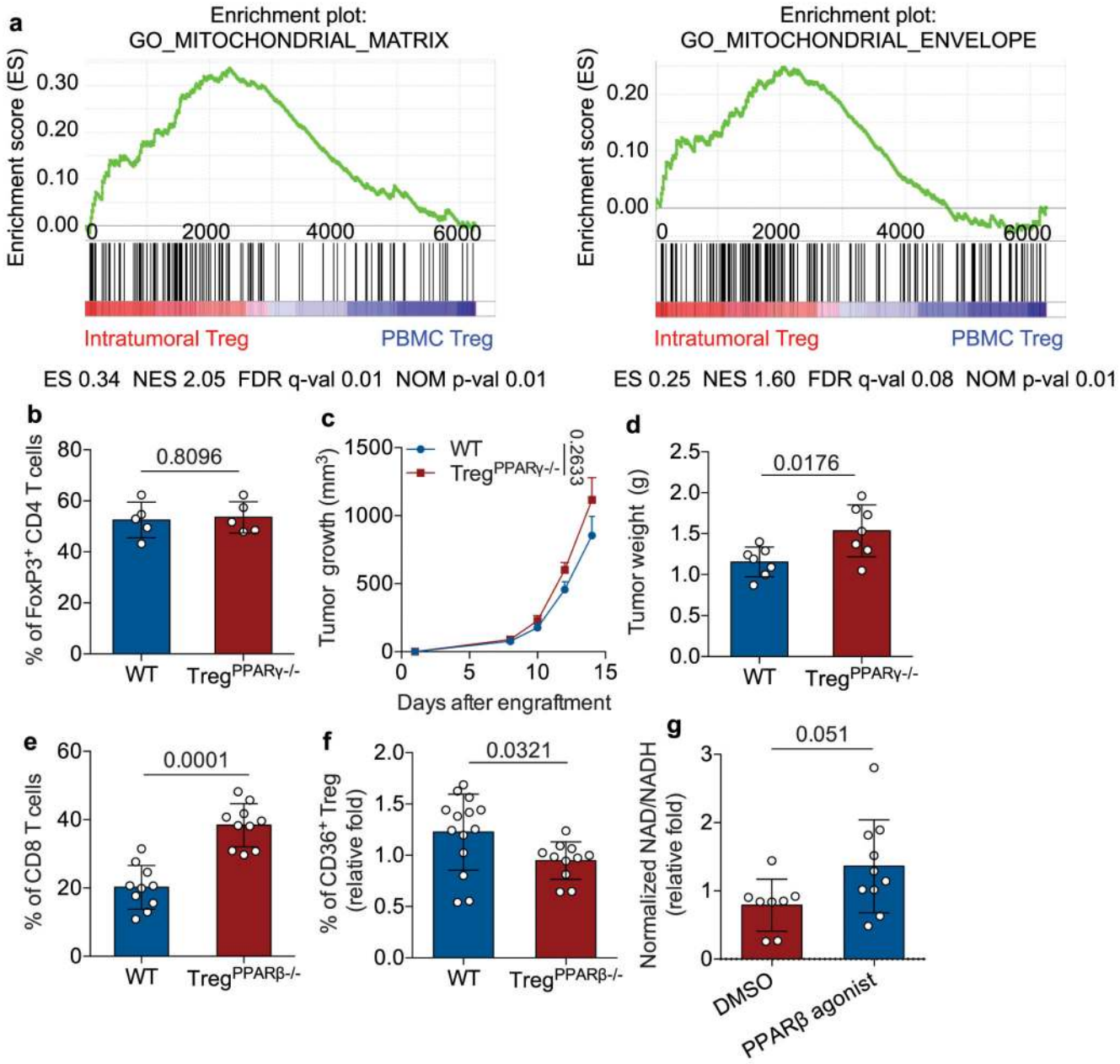

Extended Data Fig. 5. Intratumoral T_{reg} cells require PPAR-β, not PPAR-γ, signaling for metabolic adaptation.

a, Enrichment plots of signals controlling mitochondrial matrix (left) and mitochondrial envelope in intratumoral T_{reg} (n=4) compared to PBMC T_{reg} cells (n=6), identified by GSEA computational method. ES: enrichment score; NES: normalized enrichment score; FDR: false discovery rate; NOM p-val: Nominal p value. **b**, **c, d,** Percentage of FoxP3$^+$ T_{reg} cells among CD4$^+$ tumor-infiltrating T lymphocytes (n=5) (**b**), tumor growth (n=5) (**c**) and tumor weight (n=7) (**d**) from tumor-bearing WT and $T_{reg}^{PPARγ-/-}$ mice. **e,** Percentage of CD8$^+$ T cells among tumor-infiltrating T cells from tumor-bearing WT and $T_{reg}^{PPARβ-/-}$ mice (n=10). **f**, Quantitative result of CD36+ intratumoral T_{reg} cells from YUMM1.7

melanoma-bearing WT and $T_{reg}^{PPAR\beta-/-}$ mice (WT, n=14; $T_{reg}^{PPAR\beta-/-}$, n=11). **g**, NAD/NADH ratio of indicated iT_{reg} cells cultured in cancer cell-conditioned medium with DMSO or PPAR-β agonist for 48h (DMSO, n=8; PPAR-β agonist, n=10). Data are representative results of at least two independent experiments with similar results (**b, c, d**) or cumulative results from at least two independent experiments (**e, f, g**). Each symbol represents one individual. Data are mean ± S.D. (**b, d, e, f, g**) or ± S.E.M. (**c**) and were analyzed by two-tailed, unpaired Student's *t*-test.

Europe PMC Funders Author Manuscripts

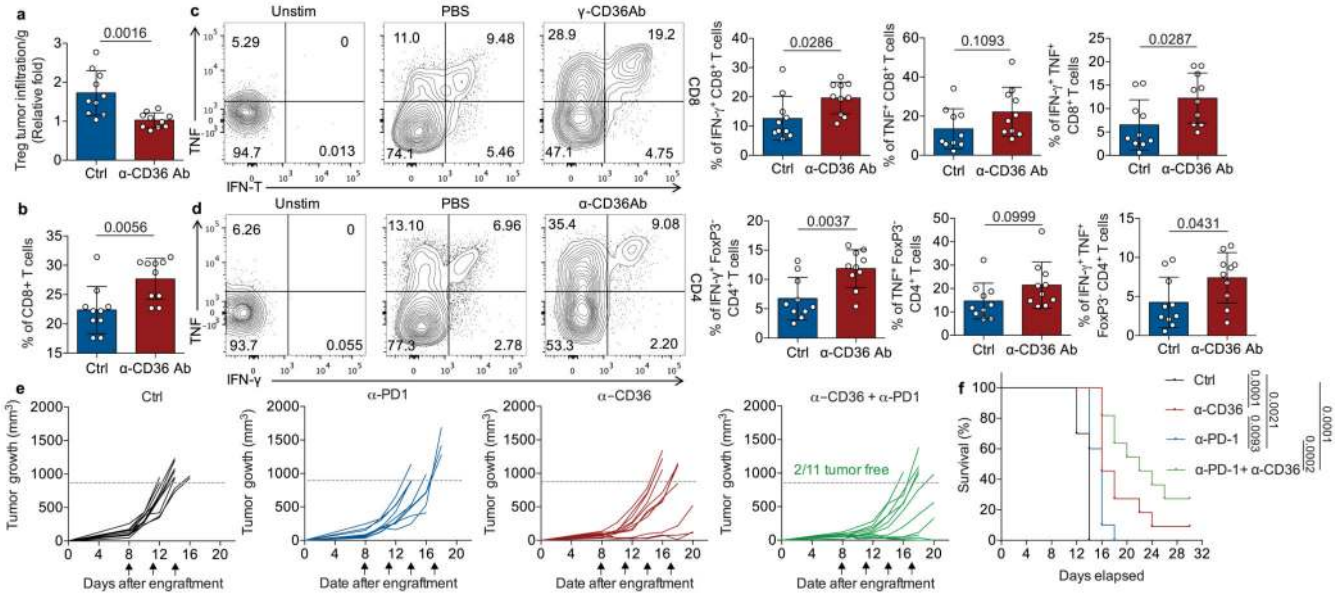

Extended Data Fig. 6. CD36-targeting unleashes host antitumor immunity.

a, b, c, d, Absolute number of FoxP3$^+$ T_{reg} cells per gram tumor (n=10 per group) (**a**), percentage of CD8$^+$ T cells among tumor-infiltrating T cells (n=10 per group) (**b**) and representative plots and percentage of indicated cytokine-producing CD8$^+$ T cells among total tumor-infiltrating CD8$^+$ T cells (**c**) and CD4$^+$ T cells among total tumor-infiltrating CD4$^+$ T cells (**d**) from YUMM1.7 melanoma-bearing mice treated with indicated treatments (n=10 per group). **e, f,** Tumor growth (**e**) and survival curves (**f**) of YUMM1.7 melanoma-bearing B6 mice treated with indicated treatments (Ctrl, n = 10; α-PD1, n = 10; α-CD36, n = 11; α-CD36 + αPD-1, n = 11). Arrows indicate the date of treatment. Dotted lines indicate the tumor volume of 800 mm^3. Data are cumulative results from at least two independent experiments. Each symbol represents one individual. Data are mean ± S.D. and were analyzed by two-tailed, unpaired Student's *t*-test (**a, b, c, d)**. Difference between survival curves was analyzed by Log-rank (Mantel-Cox) test (**f**).

Acknowledgments

We thank L.-F. Lu and W.-L. Lo for critical reading and comments for this study. We also thank Y. Maeda and H. Nishikawa for helpful discussion. P.-C.H. was supported in part by the SNSF project grants (31003A_163204 and 31003A_182470), the Swiss Cancer Foundation (KFS-3949-08-2016), the Swiss Institute for Experimental Cancer Research (ISREC 26075483), European Research Council Staring Grant (802773-MitoGuide), the Cancer Research Institute-Clinic and Laboratory Integration Program award, and the SITC-MRA Young Investigator Award. C.J. is supported by SNSF project grants (PMPDP3_129022 and PZ00P3_161459). A.Z. is supported by SNSF project grant (320030_162575) and Cancer League Switzerland (KFS-3394-02-2014). R.S. and I.G. are supported by NIH funding (P01 HL46403, P01 HL087018 and R01 HL142152 to R.S. and HL45095 and HL073029 to I.G.). E.M. acknowledges funding from the Swiss Cancer Research Foundation (KFS-3681-08-2015-R). S.M.F. acknowledges funding from FWO grant and projects as well as KU Leuven Methusalem co-funding. J.F.G. is supported by a FWO postdoctoral fellowship. J.D.W and T.M. are supported by NIH funding (P30 CA008748 and R01 CA 056821), the Swim Across America, Ludwig Institute for Cancer Research, Parker Institute for Cancer Immunotherapy and Breast Cancer Research Foundation. R.Z. is supported by the Parker Institute for Cancer Immunotherapy Bridge Scholar Award. We also appreciate the support provided by Electron Microscopy Facility at University of Lausanne and Biomedical Sequencing Facility at Research Center for Molecular Medicine of the Austrian Academy of Sciences.

Europe PMC Funders Author Manuscripts

Europe PMC Funders Author Manuscripts

References

1. Roychoudhuri R, Eil RL, Restifo NP. The interplay of effector and regulatory T cells in cancer. Current opinion in immunology. 2015; 33:101–111. DOI: 10.1016/j.coi.2015.02.003 [PubMed: 25728990]
2. Delgoffe GM, et al. Stability and function of regulatory T cells is maintained by a neuropilin-1-semaphorin-4a axis. Nature. 2013; 501:252–256. DOI: 10.1038/nature12428 [PubMed: 23913274]
3. Saito T, et al. Two FOXP3(+)CD4(+) T cell subpopulations distinctly control the prognosis of colorectal cancers. Nat Med. 2016; 22:679–684. DOI: 10.1038/nm.4086 [PubMed: 27111280]
4. Rech AJ, et al. CD25 blockade depletes and selectively reprograms regulatory T cells in concert with immunotherapy in cancer patients. Sci Transl Med. 2012; 4:134ra162.doi: 10.1126/scitranslmed.3003330
5. Sutmuller RP, et al. Synergism of cytotoxic T lymphocyte-associated antigen 4 blockade and depletion of CD25(+) regulatory T cells in antitumor therapy reveals alternative pathways for suppression of autoreactive cytotoxic T lymphocyte responses. J Exp Med. 2001; 194:823–832. DOI: 10.1084/jem.194.6.823 [PubMed: 11560997]
6. Marabelle A, et al. Depleting tumor-specific Treg cells at a single site eradicates disseminated tumors. The Journal of clinical investigation. 2013; 123:2447–2463. DOI: 10.1172/JCI64859 [PubMed: 23728179]
7. Teng MW, et al. Conditional regulatory T-cell depletion releases adaptive immunity preventing carcinogenesis and suppressing established tumor growth. Cancer Res. 2010; 70:7800–7809. DOI: 10.1158/0008-5472.CAN-10-1681 [PubMed: 20924111]
8. Walter S, et al. Multipeptide immune response to cancer vaccine IMA901 after single-dose cyclophosphamide associates with longer patient survival. Nature medicine. 2012; 18:1254–1261. DOI: 10.1038/nm.2883
9. Nishikawa H, Sakaguchi S. Regulatory T cells in tumor immunity. International journal of cancer. 2010; 127:759–767. DOI: 10.1002/ijc.25429 [PubMed: 20518016]
10. Simpson TR, et al. Fc-dependent depletion of tumor-infiltrating regulatory T cells co-defines the efficacy of anti-CTLA-4 therapy against melanoma. J Exp Med. 2013; 210:1695–1710. DOI: 10.1084/jem.20130579 [PubMed: 23897981]
11. Curtin JF, et al. Treg depletion inhibits efficacy of cancer immunotherapy: implications for clinical trials. PLoS One. 2008; 3:e1983.doi: 10.1371/journal.pone.0001983 [PubMed: 18431473]
12. Arce Vargas F, et al. Fc Effector Function Contributes to the Activity of Human Anti-CTLA-4 Antibodies. Cancer Cell. 2018; 33:649–663 e644. DOI: 10.1016/j.ccell.2018.02.010 [PubMed: 29576375]
13. Miragaia RJ, et al. Single-Cell Transcriptomics of Regulatory T Cells Reveals Trajectories of Tissue Adaptation. Immunity. 2019; 50:493–504 e497. DOI: 10.1016/j.immuni.2019.01.001 [PubMed: 30737144]
14. Arpaia N, et al. A Distinct Function of Regulatory T Cells in Tissue Protection. Cell. 2015; 162:1078–1089. DOI: 10.1016/j.cell.2015.08.021 [PubMed: 26317471]
15. Burzyn D, et al. A special population of regulatory T cells potentiates muscle repair. Cell. 2013; 155:1282–1295. DOI: 10.1016/j.cell.2013.10.054 [PubMed: 24315098]
16. Cipolletta D, et al. PPAR-gamma is a major driver of the accumulation and phenotype of adipose tissue Treg cells. Nature. 2012; 486:549–553. DOI: 10.1038/nature11132 [PubMed: 22722857]
17. Panduro M, Benoist C, Mathis D. Tissue Treg cells. Annu Rev Immunol. 2016; 34:609–633. DOI: 10.1146/annurev-immunol-032712-095948 [PubMed: 27168246]
18. Vignali DA, Collison LW, Workman CJ. How regulatory T cells work. Nat Rev Immunol. 2008; 8:523–532. DOI: 10.1038/nri2343 [PubMed: 18566595]
19. Chaudhry A, Rudensky AY. Control of inflammation by integration of environmental cues by regulatory T cells. J Clin Invest. 2013; 123:939–944. DOI: 10.1172/JCI57175 [PubMed: 23454755]
20. Campbell DJ, Koch MA. Phenotypical and functional specialization of FOXP3+ regulatory T cells. Nat Rev Immunol. 2011; 11:119–130. DOI: 10.1038/nri2916 [PubMed: 21267013]

21. Zeng H, et al. mTORC1 couples immune signals and metabolic programming to establish T(reg)-cell function. Nature. 2013; 499:485–490. DOI: 10.1038/nature12297 [PubMed: 23812589]
22. Yang K, et al. Homeostatic control of metabolic and functional fitness of Treg cells by LKB1 signalling. Nature. 2017; 548:602–606. DOI: 10.1038/nature23665 [PubMed: 28847007]
23. Huynh A, et al. Control of PI(3) kinase in Treg cells maintains homeostasis and lineage stability. Nat Immunol. 2015; 16:188–196. DOI: 10.1038/ni.3077 [PubMed: 25559257]
24. Gerriets VA, et al. Foxp3 and Toll-like receptor signaling balance Treg cell anabolic metabolism for suppression. Nat Immunol. 2016; 17:1459–1466. DOI: 10.1038/ni.3577 [PubMed: 27695003]
25. Weinberg SE, et al. Mitochondrial complex III is essential for suppressive function of regulatory T cells. Nature. 2019; 565:495–499. DOI: 10.1038/s41586-018-0846-z [PubMed: 30626970]
26. Angelin A, et al. Foxp3 Reprograms T Cell Metabolism to Function in Low-Glucose, High-Lactate Environments. Cell Metab. 2017; 25:1282–1293 e1287. DOI: 10.1016/j.cmet.2016.12.018 [PubMed: 28416194]
27. Wang H, Franco F, Ho PC. Metabolic Regulation of Treg cells in Cancer: Opportunities for Immunotherapy. Trends Cancer. 2017; 3:583–592. DOI: 10.1016/j.trecan.2017.06.005 [PubMed: 28780935]
28. Li X, et al. Navigating metabolic pathways to enhance antitumour immunity and immunotherapy. Nat Rev Clin Oncol. 2019; doi: 10.1038/s41571-019-0203-7
29. Plitas G, et al. Regulatory T Cells Exhibit Distinct Features in Human Breast Cancer. Immunity. 2016; 45:1122–1134. DOI: 10.1016/j.immuni.2016.10.032 [PubMed: 27851913]
30. Piconese S, et al. Human OX40 tunes the function of regulatory T cells in tumor and nontumor areas of hepatitis C virus-infected liver tissue. Hepatology. 2014; 60:1494–1507. DOI: 10.1002/hep.27188 [PubMed: 24756990]
31. Zappasodi R, et al. Rational design of anti-GITR-based combination immunotherapy. Nat Med. 2019; 25:759–766. DOI: 10.1038/s41591-019-0420-8 [PubMed: 31036879]
32. He N, et al. Metabolic control of regulatory T cell (Treg) survival and function by Lkb1. Proc Natl Acad Sci U S A. 2017; 114:12542–12547. DOI: 10.1073/pnas.1715363114 [PubMed: 29109251]
33. Beier UH, et al. Essential role of mitochondrial energy metabolism in Foxp3(+) T-regulatory cell function and allograft survival. FASEB J. 2015; 29:2315–2326. DOI: 10.1096/fj.14-268409 [PubMed: 25681462]
34. Ho PC, et al. Phosphoenolpyruvate Is a Metabolic Checkpoint of Anti-tumor T Cell Responses. Cell. 2015; 162:1217–1228. DOI: 10.1016/j.cell.2015.08.012 [PubMed: 26321681]
35. Siska PJ, Rathmell JC. T cell metabolic fitness in antitumor immunity. Trends Immunol. 2015; 36:257–264. DOI: 10.1016/j.it.2015.02.007 [PubMed: 25773310]
36. Vannini N, et al. The NAD-Booster Nicotinamide Riboside Potently Stimulates Hematopoiesis through Increased Mitochondrial Clearance. Cell Stem Cell. 2019; 24:405–418 e407. DOI: 10.1016/j.stem.2019.02.012 [PubMed: 30849366]
37. Ravnskjaer K, et al. PPARdelta is a fatty acid sensor that enhances mitochondrial oxidation in insulin-secreting cells and protects against fatty acid-induced dysfunction. J Lipid Res. 2010; 51:1370–1379. DOI: 10.1194/jlr.M001123 [PubMed: 19965574]
38. Morino K, et al. Regulation of mitochondrial biogenesis by lipoprotein lipase in muscle of insulin-resistant offspring of parents with type 2 diabetes. Diabetes. 2012; 61:877–887. DOI: 10.2337/db11-1391 [PubMed: 22368174]
39. Fan W, et al. PPARdelta Promotes Running Endurance by Preserving Glucose. Cell Metab. 2017; 25:1186–1193 e1184. DOI: 10.1016/j.cmet.2017.04.006 [PubMed: 28467934]
40. Pascual G, et al. Targeting metastasis-initiating cells through the fatty acid receptor CD36. Nature. 2017; 541:41–45. DOI: 10.1038/nature20791 [PubMed: 27974793]
41. Ladanyi A, et al. Adipocyte-induced CD36 expression drives ovarian cancer progression and metastasis. Oncogene. 2018; 37:2285–2301. DOI: 10.1038/s41388-017-0093-z [PubMed: 29398710]
42. Miska J, et al. HIF-1alpha Is a Metabolic Switch between Glycolytic-Driven Migration and Oxidative Phosphorylation-Driven Immunosuppression of Treg cells in Glioblastoma. Cell Rep. 2019; 27:226–237 e224. DOI: 10.1016/j.celrep.2019.03.029 [PubMed: 30943404]

43. Phan AT, Goldrath AW, Glass CK. Metabolic and Epigenetic Coordination of T Cell and Macrophage Immunity. Immunity. 2017; 46:714–729. DOI: 10.1016/j.immuni.2017.04.016 [PubMed: 28514673]
44. Liu PS, Ho PC. Mitochondria: A master regulator in macrophage and T cell immunity. Mitochondrion. 2018; 41:45–50. DOI: 10.1016/j.mito.2017.11.002 [PubMed: 29146487]
45. Pacella I, et al. Fatty acid metabolism complements glycolysis in the selective regulatory T cell expansion during tumor growth. Proc Natl Acad Sci U S A. 2018; 115:E6546–E6555. DOI: 10.1073/pnas.1720113115 [PubMed: 29941600]
46. Son NH, et al. Endothelial cell CD36 optimizes tissue fatty acid uptake. J Clin Invest. 2018; 128:4329–4342. DOI: 10.1172/JCI99315 [PubMed: 30047927]
47. Dammone G, et al. PPARgamma Controls Ectopic Adipogenesis and Cross-Talks with Myogenesis During Skeletal Muscle Regeneration. International journal of molecular sciences. 2018; 19doi: 10.3390/ijms19072044
48. Meeth K, Wang JX, Micevic G, Damsky W, Bosenberg MW, et al. The YUMM lines: a series of congenic mouse melanoma cell lines with defined genetic alterations. Pigment cell & melanoma research. 2016; 29:590–597. DOI: 10.1111/pcmr.12498 [PubMed: 27287723]
49. Ho PC, et al. Immune-based antitumor effects of BRAF inhibitors rely on signaling by CD40L and IFNgamma. Cancer Res. 2014; 74:3205–3217. DOI: 10.1158/0008-5472.CAN-13-3461 [PubMed: 24736544]
50. Driscoll WS, Vaisar T, Tang J, Wilson CL, Raines EW. Macrophage ADAM17 deficiency augments CD36-dependent apoptotic cell uptake and the linked anti-inflammatory phenotype. Circulation research. 2013; 113:52–61. DOI: 10.1161/CIRCRESAHA.112.300683 [PubMed: 23584255]
51. Cheng WC, et al. Uncoupling protein 2 reprograms the tumor microenvironment to support the anti-tumor immune cycle. Nat Immunol. 2019; 20:206–217. DOI: 10.1038/s41590-018-0290-0 [PubMed: 30664764]
52. Picelli S, et al. Full-length RNA-seq from single cells using Smart-seq2. Nature protocols. 2014; 9:171–181. DOI: 10.1038/nprot.2014.006 [PubMed: 24385147]
53. Nelson JW, Sklenar J, Barnes AP, Minnier J. The START App: a web-based RNAseq analysis and visualization resource. Bioinformatics. 2017; 33:447–449. DOI: 10.1093/bioinformatics/btw624 [PubMed: 28171615]
54. Liu PS, et al. alpha-ketoglutarate orchestrates macrophage activation through metabolic and epigenetic reprogramming. Nat Immunol. 2017; 18:985–994. DOI: 10.1038/ni.3796 [PubMed: 28714978]

Europe PMC Funders Author Manuscripts

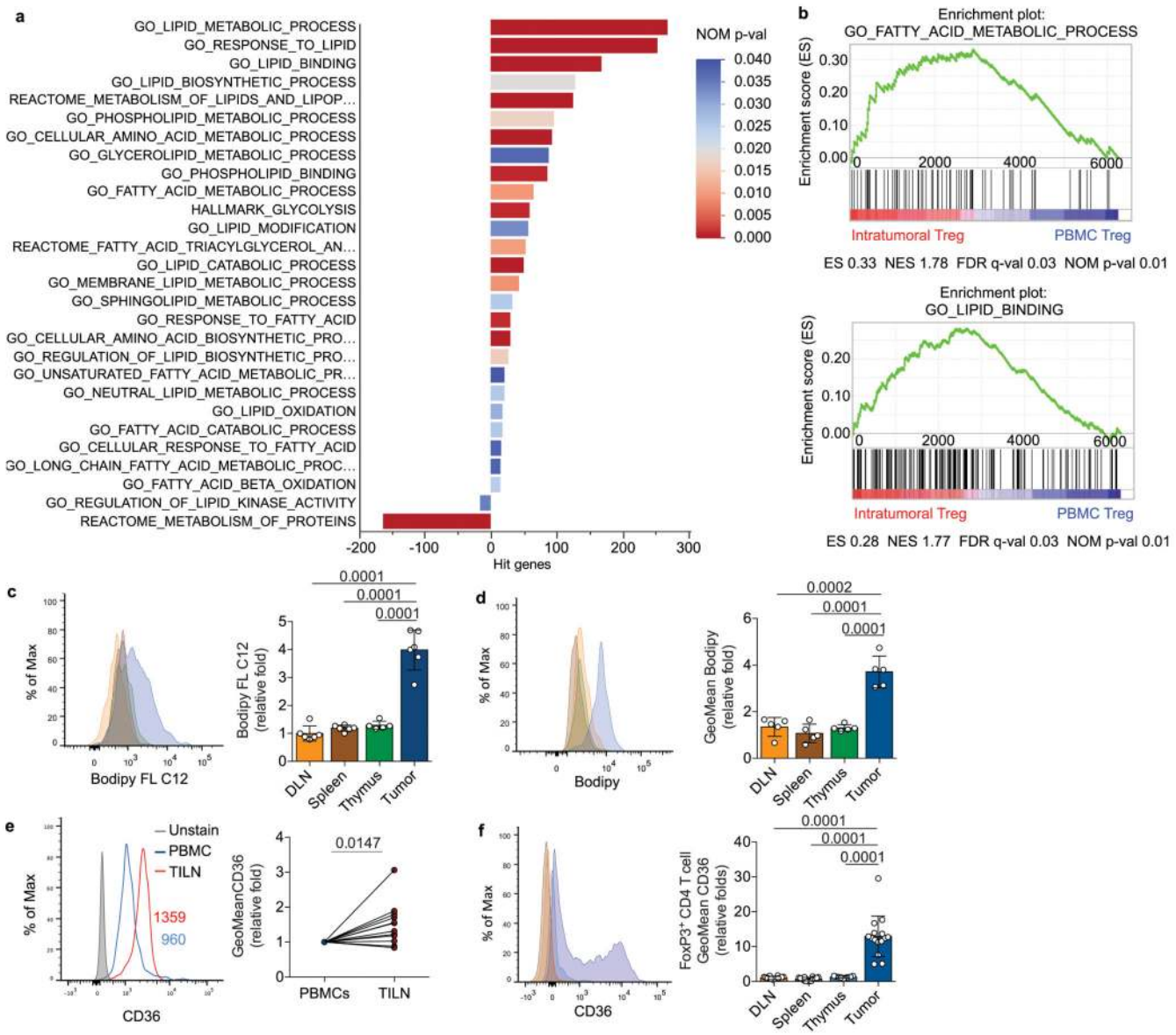

Fig. 1. Intratumoral T_{reg} cells elevates expression of CD36 and genes involved in lipid metabolism.

a, Pathway enrichment analysis focusing on metabolic machineries for RNA expression in T_{reg} cells from breast cancers (n=4) and PBMC (n=6) of breast cancer patients. Pathways with significant differential expression between intratumoral and PBMC T_{reg} cells (Nominal p value<0.05) were presented based on gene hit size. **b,** Enrichment plots of fatty acid metabolic process (top) and lipid binding (bottom) pathways in intratumoral T_{reg} cell compared to PBMC T_{reg} cells, identified by gene set enrichment analysis (GSEA) computational method. Columns indicate individual samples, and rows are each gene. Red represents a high expression level, and blue indicates a low expression level. **c, d,** Representative histogram (left) and quantitative results of geometric mean (GeoMean) fluorescent intensity (right) of Bodipy FL C12 (n=6, one outlier was removed from the thymus group) (**c**) and Bodipy 493/503 (Bodipy) (n=5) (**d**) in T_{reg} cells from indicated

Europe PMC Funders Author Manuscripts

Europe PMC Funders Author Manuscripts

tissues of Yumm1.7 melanoma-bearing B6 mice. DLN: draining lymph node; spleen; thymus; tumor. **e, f,** Representative histogram (left) and quantitative results of geometric mean (GeoMean) fluorescent intensity of CD36 surface staining in T_{reg} cells from PBMC and tumor infiltrated lymph nodes (TILNs) of melanoma patients (n=12) (**e**) and from indicated tissues of Yumm1.7 melanoma-bearing B6 mice (DLN, n=15; spleen, n=15; thymus, n=9; tumor, n=15) (**f**). TILs: tumor-infiltrating lymphocytes. Data are representative results of three independent experiments with similar results (**c, d**) or cumulative results from three independent experiments (**e, f**). Each symbol represents one individual. ES: enrichment score; NES: normalized enrichment score; FDR: false discovery rate; NOM p-val: Nominal p value. Data are mean ± S.D. and were analyzed by two-tailed, unpaired Student's *t*-test (**c, d, f**) or by two-tailed, paired Student's *t*-test (**e**).

Europe PMC Funders Author Manuscripts

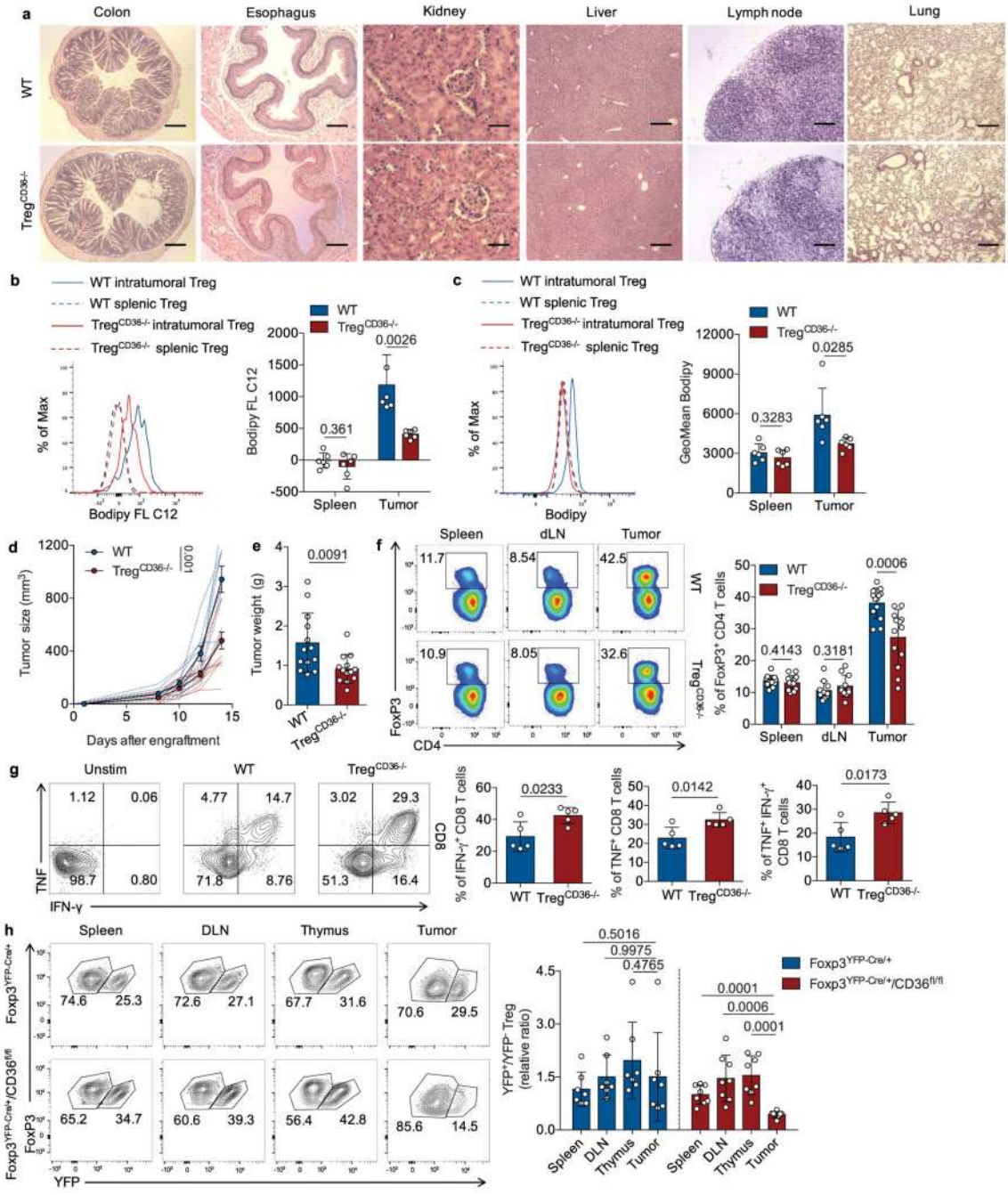

Fig. 2. Disruption of CD36 selectively impairs the accumulation and suppressive function of intratumoral T_{reg} cells.

a, Representative images of haematoxylin and eosin (H&E) staining for indicated tissues from wild-type (WT) or $T_{reg}^{Cd36-/-}$ mice at the age of 21-23 weeks. Scale bar, 200 μm. **b, c,** Representative histogram (left) and quantitative results of geometric mean (GeoMean) fluorescent intensity (right) of Bodipy FL C12 (**b**) and Bodipy 493/503 (**c**) in splenic and intratumoral T_{reg} cells from Yumm1.7 melanoma-bearing WT or $T_{reg}^{CD36-/-}$ mice (n=6 per group). **d, e,** Tumor growth (WT, n=9; $T_{reg}^{Cd36-/-}$, n=10) (**d**) and tumor weight (n=13) (**e**) of

YUMM1.7 melanoma from WT or $T_{reg}^{Cd36-/-}$ mice. *Foxp3*$^{YFP\text{-}Cre}$ mice were used as WT mice. **f,** Representative plots (left) and percentage of FoxP3$^+$ T_{reg} cells among CD4$^+$ T cells in indicated tissues of tumor-bearing WT and $T_{reg}^{Cd36-/-}$ mice (spleen and tumor n=13; dLN, n=11). **g,** Representative plots (left) and percentage of indicated cytokine-producing CD8$^+$ T cells among total tumor-infiltrating CD8$^+$ T cells from indicated mice (right) (n=5 per group). **h,** Representative plots (left) and quantitative ratios (right) of CD36-deficient/WT T_{reg} cells in tumors and indicated tissues from either *Foxp3*$^{YFP\text{-}Cre/+}$/*Cd36*$^{fl/fl}$ female mice (n=8) or *Foxp3*$^{YFP\text{-}Cre/+}$ female mice (n=7). Data are representative result of two independent experiments with similar results (**b, c, g**) or cumulative results from at least two independent experiments (**d, e, f, h**). Each symbol represents one individual. Data are mean ± S.D. (**b, c, e, f, g, h**) or ± S.E.M. (**d**) and were analyzed by two-tailed, unpaired Student's *t*-test (**b, c, d, e, f, g, h**).

Europe PMC Funders Author Manuscripts

Europe PMC Funders Author Manuscripts

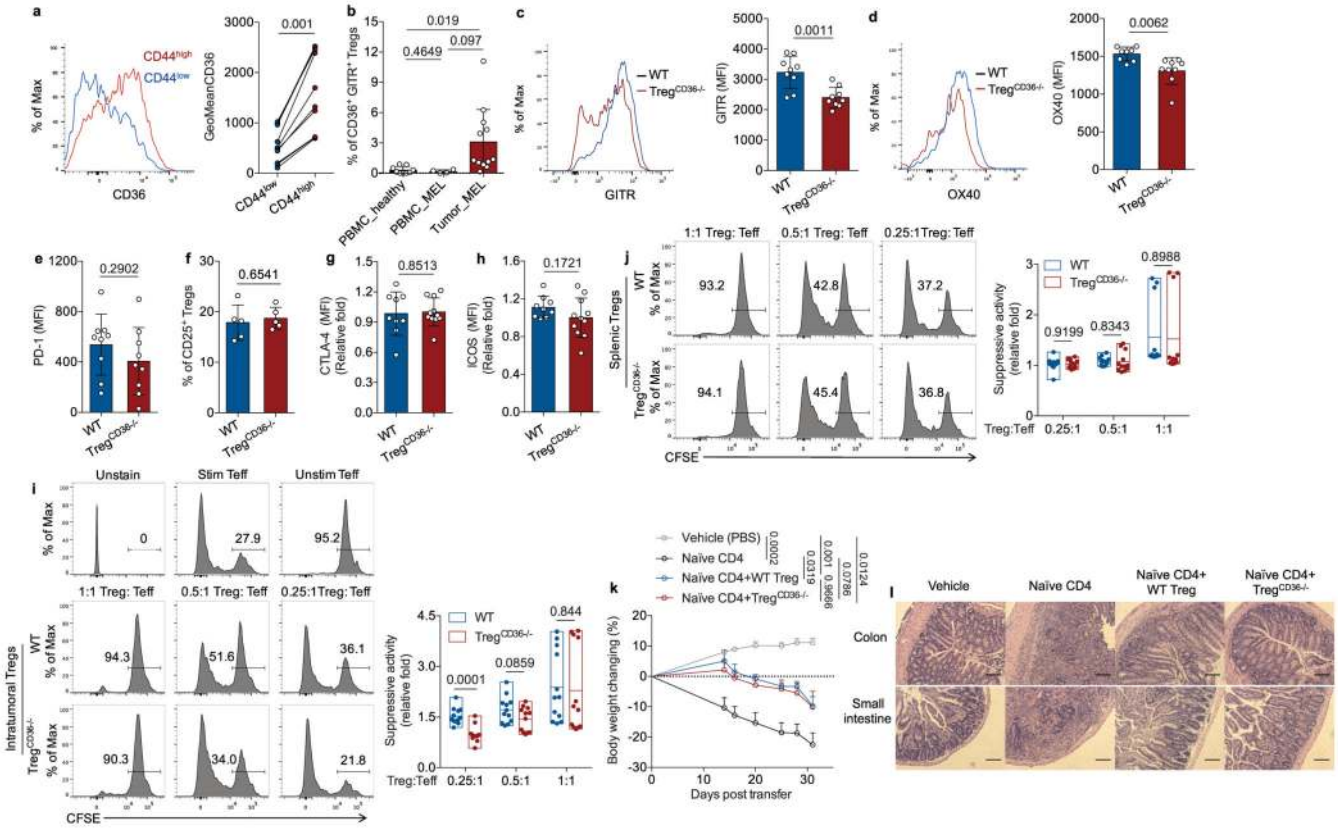

Fig. 3. CD36 expression selectively supports suppressive activity of intratumoral T_{reg} cells.

a, Representative histogram (left) and quantitative results of geometric mean (GeoMean) fluorescent intensity (right) of CD36 in $CD44^{lo}$ and $CD44^{hi}$ intratumoral T_{reg} cells from Yumm1.7 melanoma-bearing WT mice (n=10). **b,** Percentage of $CD36^+$ T_{reg} cells among $GITR^+/FoxP3^+$ T_{reg} cells of PBMCs from healthy donors (n=9) or melanoma patients (n=4) or TILs from melanoma patients (n=12). **c, d,** Representative histograms and quantitative results of geometric mean fluorescent intensity (MFI) of GITR (**c**) and OX40 (**d**) in intratumoral T_{reg} cells from indicated mice (n=9 per group, one outlier was removed from OX40_WT group). **e, f, g, h,** Expression of PD-1 in intratumoral T_{reg} cells (n=9 per group) (**e**), percentage of $CD25^+/FoxP3^+$ T_{reg} cells among total intratumoral T_{reg} cells population (n=5 per group) (**f**), and expression of CTLA-4 (**g**) and ICOS (**h**) ($Foxp3^{YFP\text{-}Cre}$, n=9; $T_{reg}^{Cd36-/-}$, n=11) in intratumoral T_{reg} cells of YUMM1.7 melanoma-bearing WT and $T_{reg}^{CD36-/-}$ mice. **i, j,** Ex vivo suppression of CFSE-labeled WT naïve $CD8^+$ T cell proliferation by WT and $T_{reg}^{Cd36-/-}$ T_{reg} cells sorted from tumors (**i**) or spleens (**j**) with annotated ratios (n=12). **k,** Body weight measurement in $Rag1^{-/-}$ mice receiving naïve $CD4^+$ T cell alone or in combination with either WT or $T_{reg}^{CD36-/-}$ T_{reg} cells (vehicle, n=4; naïve CD4, n=7; WT T_{reg}, n=6; $T_{reg}^{Cd36-/-}$, n=6). **l,** Representative images of haematoxylin and eosin (H&E) staining of colon and small intestine from indicated group of $Rag1^{-/-}$ mice. Scale bar, 200 μm. Data are representative result of three independent experiments with similar results (**l, f**) or cumulative results from at least two independent experiments (**a, b, c, d, e, g, h, i, j, k**). Each symbol represents one individual. Data are mean ± S.D. (**a, b, c, d, e,**

f, g, h, i, j) or ± S.E.M. (**k**) and were analyzed by two-tailed, unpaired Student's *t*-test (**b, c, d, e, f, g, h, i, j, k**) or two-tailed, paired Student's *t*-test (**a**).

Europe PMC Funders Author Manuscripts

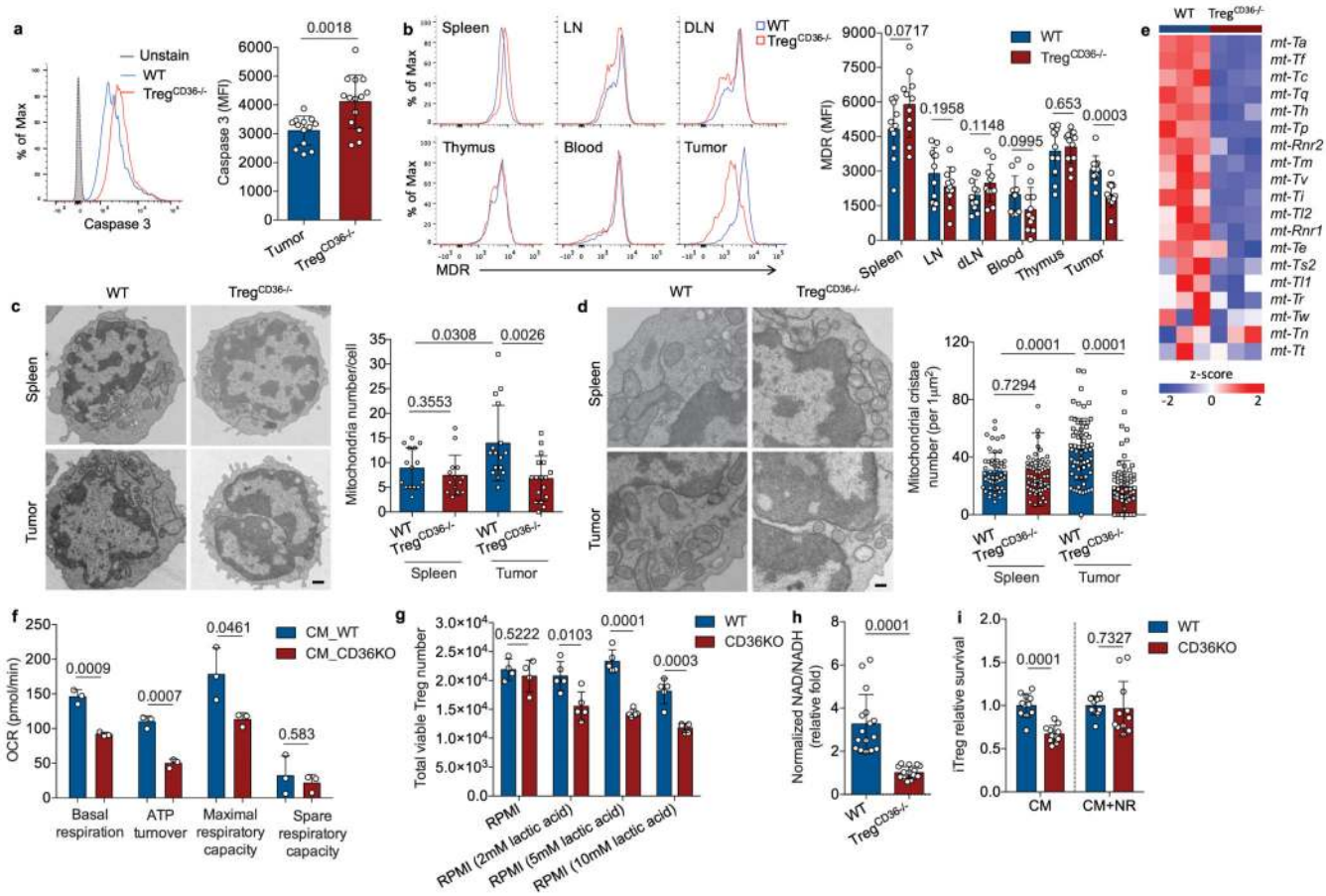

Fig. 4. CD36 deficiency stimulates apoptosis in intratumoral T_{reg} cells.

a, Representative histograms (left) and quantitative analysis (right) of cleaved caspase-3 levels in intratumoral T_{reg} cells from WT (n=13) and $T_{reg}^{Cd36-/-}$ tumor-bearing mice (n=14). **b,** Representative histograms (left) and quantitative analysis (right) of MitoTracker Deep Red (MDR) staining in T_{reg} cells of spleen, non-draining lymph node (LN), draining lymph node (DLN), blood, thymus, and tumor from tumor-bearing WT and $T_{reg}^{Cd36-/-}$ mice (n=11 per group). **c, d,** Representative electron microscope images (left) and quantitative plots (right) of mitochondrion number (**c**) and crista density (**d**) in splenic and intratumoral T_{reg} cells from tumor-bearing WT and $T_{reg}^{Cd36-/-}$ mice. Photo of individual cells was taken with EM for the mitochondrial calculation (WT spleen, n=15; WT tumor, n=16, $T_{reg}^{Cd36-/-}$ spleen, n=14; $T_{reg}^{Cd36-/-}$ tumor, n=17). Scale bars: 500 nm in (**c**) and 200 nm in (**d**). **e,** Expression of genes encoding mitochondrial tRNAs in WT and $T_{reg}^{Cd36-/-}$ intratumoral T_{reg} cells, assessed by RNA-seq (n=3 per group). **f,** OCR of indicated iT_{reg} cell cultured in cancer cell-conditioned medium for 48 hrs (n=3 per group). **g,** The viability of either WT or $T_{reg}^{Cd36-/-}$ iT_{reg} cell cultured in cancer cell-conditioned medium as above and then treated with indicated concentration of lactic acids for another 72 hrs (n=4 in RPMI group; n=5 in other groups). **h,** NAD/NADH ratio of indicated iT_{reg} cell cultured in cancer cell-conditioned medium for 48 hrs (n=16). **i,** Relative viability of either WT or $T_{reg}^{Cd36-/-}$ iT_{reg} cells treated with cancer cell-conditioned medium with or without NR (400 μM) for 72 hrs (n=11 per group). Results were normalized to the survival cells of control treatment in

Europe PMC Funders Author Manuscripts

indicated group. NR: nicotinamide riboside. Data are representative result of three independent experiments with similar results (**f, g**) or cumulative results of three independent experiments (**a, b, e, h, i**). Data are mean ± S.D. and were analyzed by two-tailed, unpaired Student's *t*-test.

Europe PMC Funders Author Manuscripts

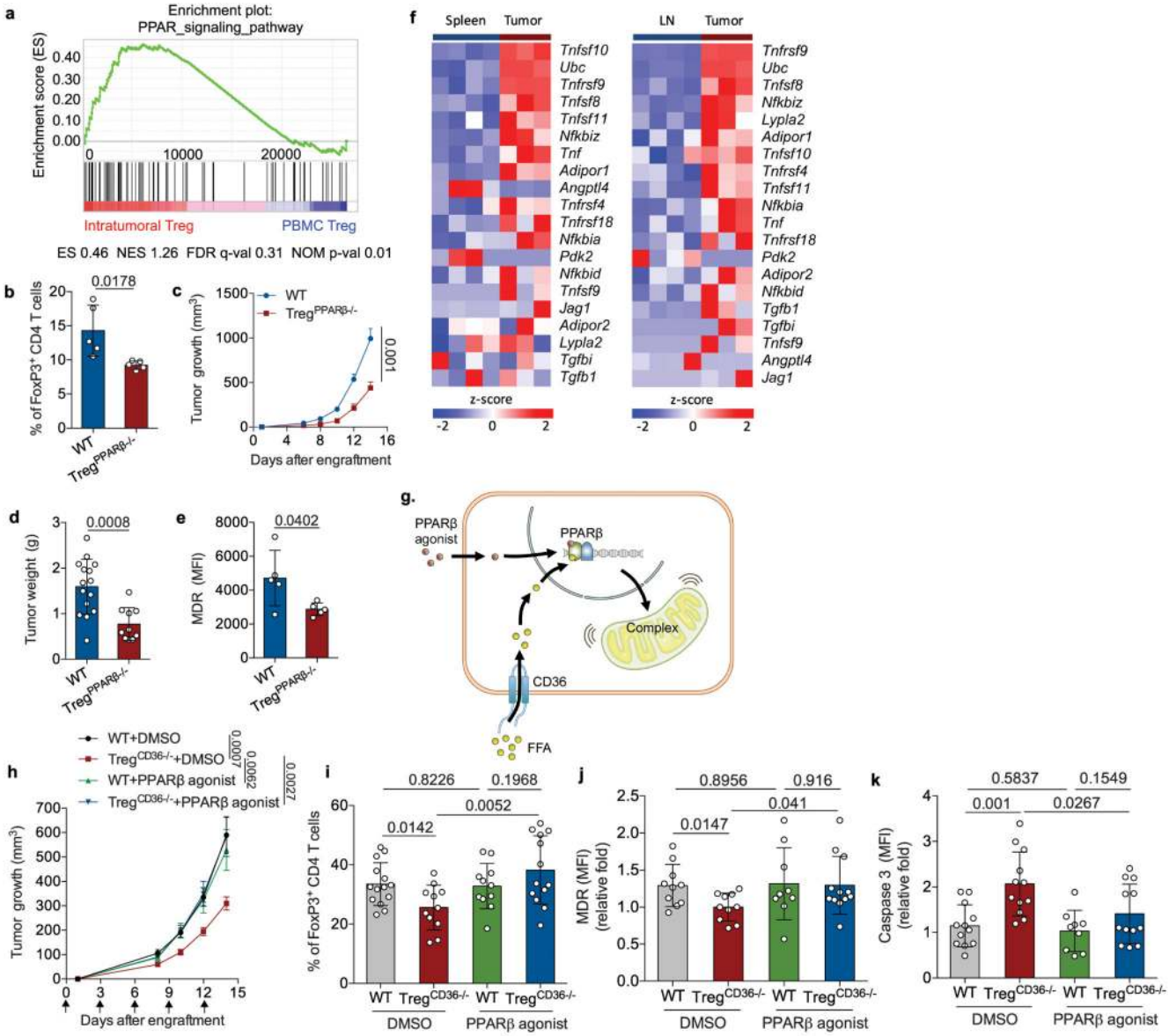

Fig. 5. PPAR-β signaling is required for metabolic adaptation in intratumoral T_{reg} cells.

a, Enrichment plots of PPAR signaling pathways in intratumoral T_{reg} cells (n=4) compared to PBMC T_{reg} cells (n=6), identified by GSEA computational method. ES: enrichment score; NES: normalized enrichment score; FDR: false discovery rate; NOM p-val: Nominal p value. **b,** Percentage of FoxP3$^+$ T_{reg} cells among CD4$^+$ tumor-infiltrating T lymphocytes from tumor-bearing WT and $T_{reg}^{PPARβ-/-}$ mice (n=5). **c, d,** Tumor growth (**c**) and tumor weight (**d**) of YUMM1.7 melanoma from WT or $T_{reg}^{PPARβ-/-}$ mice (WT, n=15; $T_{reg}^{Cd36-/-}$, n=10). *Foxp3*$^{YFP-Cre}$ mice were used as WT mice. **e,** Quantitative result of geometric MFI of MDR staining in intratumoral T_{reg} cells from WT and $T_{reg}^{PPARβ-/-}$ mice (n=5 per group). **f,** Expression of target genes of PPAR-β in T_{reg} cells from spleens, draining lymph nodes (LN) and tumor, assessed by RNA-seq. **g,** Illustration of postulated signaling cascade and the rationale for applying PPAR-β agonist in $T_{reg}^{Cd36-/-}$ mice. **h, i,** WT and $T_{reg}^{Cd36-/-}$ mice

Europe PMC Funders Author Manuscripts

were engrafted with YUMM1.7 melanoma cells and then treated with either DMSO or PPARβ agonist as described in methods. Tumor growth (WT+DMSO, n=6; $T_{reg}^{Cd36-/-}$ +DMSO, n=11; WT+PPAR-β agonist, n=5; $T_{reg}^{Cd36-/-}$+PPAR-β agonist, n=9) (**h**) and percentage of FoxP3$^+$ T_{reg} cells among CD4$^+$ tumor-infiltrating T lymphocytes (WT +DMSO, n=14; $T_{reg}^{Cd36-/-}$+DMSO, n=11; WT+PPAR-β agonist, n=11; $T_{reg}^{Cd36-/-}$+PPAR-β agonist, n=13) (**i**) were analyzed. **j, k,** Quantitative analysis of MitoTracker Deep Red (MDR) staining (DMSO, n=10; PPAR-β agonist, n=12) (**j**) and expression of cleaved caspase-3 (**k**) in intratumoral T_{reg} cells of WT and $T_{reg}^{Cd36-/-}$ mice treated with indicated treatments (n=9 in WT+PPAR-β agonist group; n=12 in other groups). Data are representative result of three independent experiments with similar results (**b, e**) or cumulative results from at least three independent experiments (**c, d, f, h, i, j, k**). Data are mean ± S.D. (**b, d, e, i, j, k**) or ± S.E.M. (**c, h**) and were analyzed by two-tailed, unpaired Student's *t*-test.

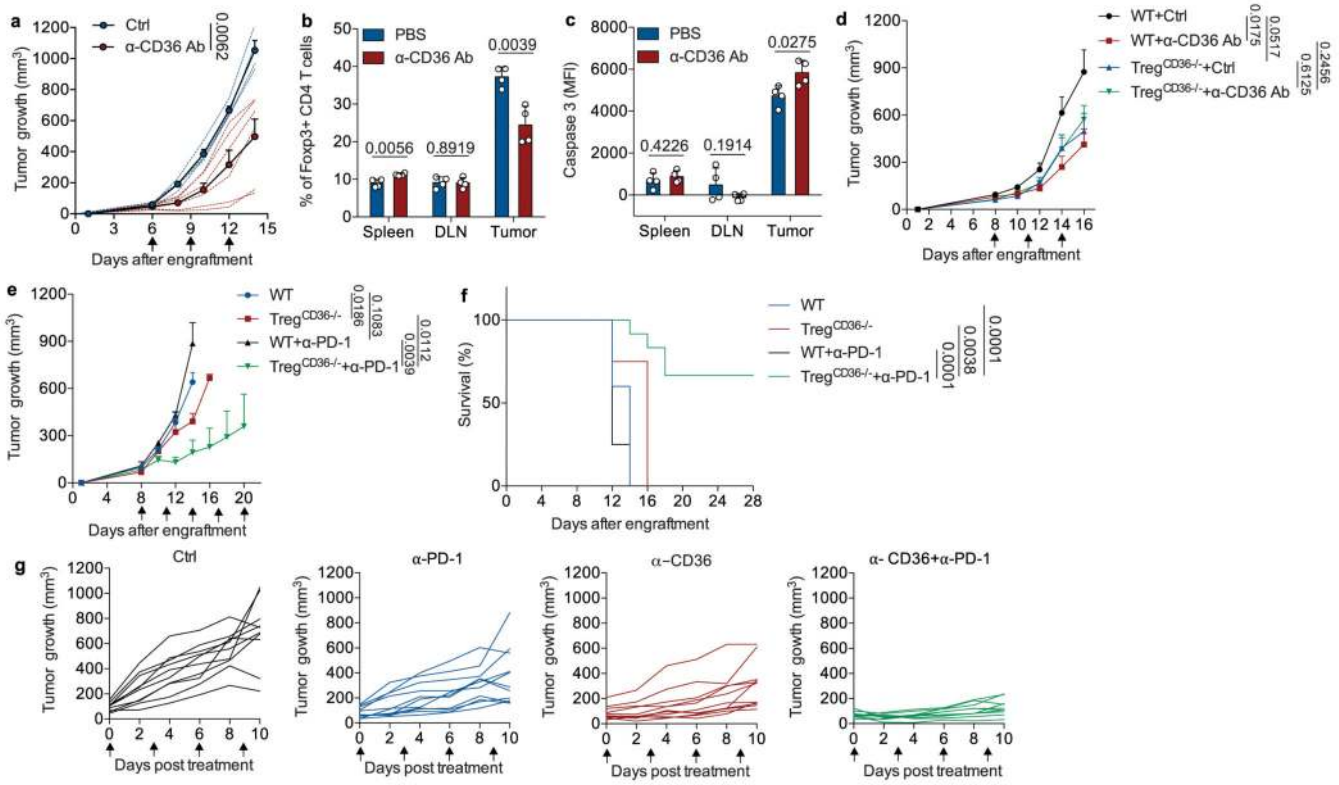

Fig. 6. CD36-targeting impairs intratumoral T_{reg} cells and primes tumors to PD-1 blockade.

a, b, c, Tumor growth (**a**) (Ctrl, n=4; α-CD36 Ab, n=6), percentage of FoxP3$^+$ T_{reg} cells among CD4$^+$ T cells of indicated tissues (n=4) (**b**), and expression of cleaved caspase-3 in T_{reg} cells isolated from indicated tissues (n=4) (**c**) of YUMM1.7 melanoma-bearing B6 mice treated with the indicated treatments. **d,** Tumor growth of YUMM1.7 melanoma-bearing WT and $T_{reg}^{Cd36-/-}$ mice treated with either control vehicle (Ctrl) or α-CD36 mAb (WT +Ctrl, n=12; WT+α-CD36 Ab, n=10; $T_{reg}^{Cd36-/-}$+Ctrl, n=11; $T_{reg}^{Cd36-/-}$+α-CD36 Ab, n=10). **e, f,** Tumor growth (**e**) and survival curves (**f**) of YUMM1.7 melanoma-bearing WT and $T_{reg}^{Cd36-/-}$ mice treated with the indicated treatments (WT, n=5; $T_{reg}^{Cd36-/-}$, n=4; WT +α-PD1, n=4; $T_{reg}^{Cd36-/-}$+α-PD1, n=4). Comparison between $T_{reg}^{Cd36-/-}$ and $T_{reg}^{Cd36-/-}$+α-PD1 was done based on the readouts on day 16 and other comparisons were done based on the readouts on day 14. **g,** Tumor growth of inducible Braf/Pten melanoma-bearing mice treated with indicated treatments (Ctrl, n = 10; α-PD1, n = 11; α-CD36, n = 11; α-CD36 + αPD-1, n = 11). Arrows indicate the date of treatment. Data are representative result of at least two independent experiments with similar results (**a, b, c, e, f**) or cumulative results from at least two independent experiments (**d, g**). Each symbol represents one individual. Data are mean ± S.D. (**b, c**) or ± S.E.M. (**a, d, e**) and were analyzed by two-tailed, unpaired Student's *t*-test. Difference between survival curves was analyzed by Log-rank (Mantel-Cox) test (**f**).

Europe PMC Funders Author Manuscripts